INFORMATION TO USERS

This was produced from a copy of a document sent to us for microfilming. While the most advanced technological means to photograph and reproduce this document have been used, the quality is heavily dependent upon the quality of the material submitted.

The following explanation of techniques is provided to help you understand markings or notations which may appear on this reproduction.

1. The sign or "target" for pages apparently lacking from the document photographed is "Missing Page(s)". If it was possible to obtain the missing page(s) or section, they are spliced into the film along with adjacent pages. This may have necessitated cutting through an image and duplicating adjacent pages to assure you of complete continuity.

2. When an image on the film is obliterated with a round black mark it is an indication that the film inspector noticed either blurred copy because of movement during exposure, or duplicate copy. Unless we meant to delete copyrighted materials that should not have been filmed, you will find a good image of the page in the adjacent frame.

3. When a map, drawing or chart, etc., is part of the material being photographed the photographer has followed a definite method in "sectioning" the material. It is customary to begin filming at the upper left hand corner of a large sheet and to continue from left to right in equal sections with small overlaps. If necessary, sectioning is continued again—beginning below the first row and continuing on until complete.

4. For any illustrations that cannot be reproduced satisfactorily by xerography, photographic prints can be purchased at additional cost and tipped into your xerographic copy. Requests can be made to our Dissertations Customer Services Department.

5. Some pages in any document may have indistinct print. In all cases we have filmed the best available copy.

KELLY, JOHN DAVID
  RADAR MEASUREMENTS OF TEMPERATURES AND IONIC
  COMPOSITION IN THE HIGH-LATITUDE IONOSPHERE.

  UNIVERSITY OF ALASKA, PH.D., 1979

RADAR MEASUREMENTS OF TEMPERATURES AND

IONIC COMPOSITION IN THE HIGH-LATITUDE IONOSPHERE

A

DISSERTATION

Presented to the Faculty of the

University of Alaska in Partial Fulfillment

of the Requirements

for the Degree of

DOCTOR OF PHILOSOPHY

by

John David Kelly

Fairbanks, Alaska

RADAR MEASUREMENTS OF TEMPERATURES AND

IONIC COMPOSITION IN THE HIGH-LATITUDE IONOSPHERE

RECOMMENDED:

Chairman, Advisory Committee

Head, Space Physics and Atmospheric
Sciences Program

Director, Geophysical Institute

APPROVED:

Dean, College of Environmental
Sciences

Date   4 – 19 - 79

Vice Chancellor for Research and
Advanced Study

Date   April 20, 1979

ABSTRACT

    The thermal and chemical structure of the thermosphere at high

latitudes is strongly influenced by auroral energy inputs. These inputs

are highly variable and will affect ionospheric circulation patterns as

well as ionic composition, electron-density distribution, and temperature

variations. This dissertation presents the first continuous ground-based

measurements of temperatures and ionic composition of the high-latitude

thermosphere in the polar region.

    The measurements were made with the incoherent-scatter radar located

at Chatanika, Alaska (L = 5.6). Previous measurements of these parameters

have been made with both rockets and satellites. The use of ground-based

radar, however, allows continuous measurement without the coverage limi-

tations of both rockets and satellites.

    In this dissertation I present the results of four continuous 24-

hour periods. The periods were selected such that conditions during

summer, winter, near summer solstice, and near autumnal equinox were sampled.

These periods were also chosen so that both active and quiet geomagnetic

conditions existed. Therefore, the variations in electron and ion temper-

atures and ion composition due to diurnal, seasonal, and auroral effects

have been examined.

iii

The temperature variations during particle precipitation and joule heating events are quite dramatic. The electron temperature increased as much as 1000 K above the neutral-gas temperature during precipitation. The ion temperature also increased by a similar amount during a large joule heating event (30 ergs/cm^2-s).

During quiet periods, the solar extreme ultraviolet radiation determines the diurnal temperature variations. For example, the F-region electron temperatures varied as much as 1000 K over the day/night cycle. The ion temperatures varied only 100 K over the same period. These quiet-time results are similar to measurements made at midlatitudes.

The term "transition altitude" is used to describe variations in the ion composition. Above this altitude, O^+ ions dominate; below this altitude, molecular ions (NO^+, O_2^+) dominate. Large electric fields were observed to have a significant effect on ion composition. In fact, the largest change in the transition altitude occurred during the large joule heating event mentioned above. The transition altitude increased at least 50 km during that period and remained elevated for several hours.

During quiet periods the variation in composition is less dramatic. In the winter, the transition altitude is near 190 km at night and near 175 km during the day. There is very little variation in the summer transition altitude (170 km) because at high latitude the solar zenith angle does not exceed about 96° and the ionospheric F-region is illuminated continuously. A seasonal variation, similar to midlatitude observations, was also observed--i.e., the daytime transition altitude is approximately 15 km lower in the winter than in the summer.

iv

ACKNOWLEDGMENTS

CONTENTS

CONTENTS (continued)

CONTENTS (concluded)

viii

LIST OF ILLUSTRATIONS (continued)

x

xi

LIST OF ILLUSTRATIONS (concluded)

LIST OF TABLES

I   INTRODUCTION

The magnetosphere has a significant effect on the high latitude thermosphere because it directs large amounts of solar energy in two forms: energetic electrons and convection electric fields. These energy inputs are highly variable and are often larger than the energy deposited at ionospheric altitudes directly by the solar extreme ultraviolet (EUV) and X-ray radiation. The resultant effects are significant—the thermospheric temperature structure and ionic composition are strongly influenced by the dissipation of the magnetospheric energy sources. Ionospheric circulation patterns also will be affected by changes in the thermal structure.

During intense particle precipitation associated with magnetospheric substorms, the electron temperature is elevated by 1000 K or more in the F-region. Similarly, ion temperatures can be as high as 2000 to 3000 K (twice the ambient temperature) during periods when large convection electric fields (60 to 100 mV/m) are present.

A number of techniques have been previously employed to measure the effects of these magnetospheric substorm manifestations. Satellite and rocket-borne instrumentation have provided most of the previous measurements of temperatures (electron and ion) and ionic composition. These measurements have a number of limitations, however. With rockets and satellites it is difficult to determine the effects on the ionosphere of large energy inputs for a number of reasons:

1

- The satellite data are limited to a single altitude at a particular location.

- The rocket data provide a single profile of the measurable parameters.

- Satellite data provide only gross temporal variation ($\sim$ 90 min period); neither satellite nor rocket data are continuous in time.

This dissertation presents the first continuous measurements of ion and electron temperatures and ionic composition at auroral latitudes. It also demonstrates the success of a technique to determine ion composition never before used at high latitudes. The measurements were performed using the incoherent scatter radar at Chatanika, Alaska (L = 5.6). The experiments were largely exploratory because analysis techniques used by incoherent-scatter radars at midlatitudes were not directly applicable and had to be adapted for use in the more complex high-latitude ionosphere. The techniques developed by Evans and Oliver [1972], Waldteuful [1971], and others for a midlatitude ionosphere were extended and modified as required by the auroral conditions.

The ground-based incoherent-scatter radar is well suited for determining both temporal and spatial variation of ionospheric parameters such as the electron density, ion velocity, electron and ion temperature, and the ionic mass, all as functions of altitude for a desired period. Briefly, the electron density is derived from the received backscattered power, the ion velocity from the Doppler shift, and the electron and ion temperatures (T_e, T_i) and ion mass (M_i) from the spectral shape of the

received signal. In a later section these parameters are discussed in detail, particularly the dependence of the spectral shape on T_e, T_i, and M_i.

Seasonal and diurnal variations in electron and ion temperatures, and ionic composition have been examined for the high-latitude ionosphere. Four 24-hour periods were chosen for detailed analysis in order to present samples of summer, winter, and near-equinox conditions. The magnetic activity varied from quiet to storm conditions in the selected data base. In addition, the effects of large energy inputs (both joule and energetic particle precipitation) on the temperature and ionic composition have been analyzed.

This dissertation is organized in the following manner:

- Section II contains a background discussion of the auroral processes and their effect on the high-latitude ionosphere. This discussion is based on theoretical works by Rees [1975], Walker and Rees [1968], and others. The effects of auroral energy input on ion composition are also discussed.

- Section III contains the following:
  - A brief description of incoherent scatter theory
  - A description of techniques used at midlatitudes for determining T_i, T_e, M_i.
  - A description of the technique adapted for high latitudes for determining T_i, T_e, M_i.

- A description of the experimental procedure

- A description of the method for determining energy

  inputs from radar-measured parameters.

- Section IV contains the data from the four 24-hour periods

  and data taken during a simultaneous rocket flight. The

  rocket carried a mass spectrometer; consequently, a com-

  parison of radar composition measurements with _in situ_

  measurements can be made.

- Section V contains the analysis and discussion of the

  temperature and ion composition data; both quiet and

  active periods are discussed. The analysis is aided by

  numerically modeling the ion composition using a simpli-

  fied system of reactions.

- Section VI contains the conclusions and recommendations

  for future research.

- The Appendix contains the error analysis.

II   BACKGROUND

The high-latitude thermosphere, in contrast with the midlatitude thermosphere, is strongly coupled to the magnetosphere. As a result, large amounts of energy and momentum are transferred from the magnetosphere to the ionosphere. These energy inputs have a significant effect on the morphology, thermodynamics, and chemistry of the high-latitude ionosphere. Energetic auroral particles are responsible for both heating effects and the production of ionization. Electric fields are responsible for joule heating. The relationship between the auroral processes and their manifestation in the high-latitude ionosphere is outlined in Figure 1.

A.   Particle Precipitation and Electron Temperature

On the left side of the auroral diagram we indicate the heating process due to auroral electrons. A flux of energetic electrons bombards the upper atmosphere, the depth of penetration depending on the electron energy. Most of the energy is deposited between 100 and 120 km. The energetic primary electrons transfer energy through the ionization of the ambient neutral constituents (N_2, O_2, and O). The collision reactions are:

$$N_2 + e \longrightarrow N_2^+ + 2e \qquad (1)$$

$$N_2 + e \longrightarrow N^+ + N + 2e \qquad (2)$$

$$O_2 + e \longrightarrow O_2^+ + 2e \qquad (3)$$

5
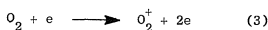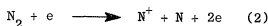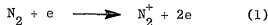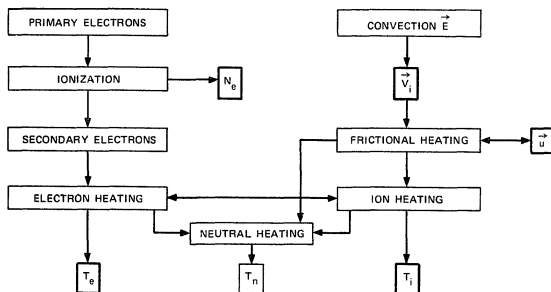
FIGURE 1   AURORAL BLOCK DIAGRAM.   Adapted from Rees [1975].

$$O_2 + e \longrightarrow O^+ + O + 2e \quad (4)$$

$$O + e \longrightarrow O^+ + 2e. \quad (5)$$
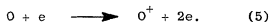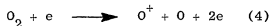
In the above ionizing reactions some of the energy from primary electrons goes into the production of excited states of N^+, O^+, N, and O. Enhanced vibrational and rotational levels of N_2^+, O_2, and O_2^+ are also produced. The secondary electrons have energies of tens of electron volts. Much of this energy is lost in inelastic collisions with neutrals and finally the remaining energy is shared with the ambient electrons producing a temperature enhancement.

Auroral zone electron temperatures have been calculated by Walker and Rees [1968] and Rees et al. [1971]. The temperature is determined by solving the electron energy equation taking into account local heating, cooling, and conduction. Examples of enhanced electron temperature profiles are shown in Figure 2. F-region temperatures near 3000 K are predicted to occur during intense precipitation periods. Measured electron temperatures are compared with those determined theoretically in Section V.

B. Joule Heating and Ion Temperature

Referring again to Figure 1, the right side indicates the process of heating by electric fields perpendicular to the magnetic field. Magnetospheric $\vec{E}$ fields are mapped down along magnetic field lines and are consequently applied to the ionosphere. The field produced $\vec{E} \times \vec{B}$ drift of both ions and electrons. As the ions drift through the neutral atmosphere they collide with neutrals and frictional heating (or joule heating) results.
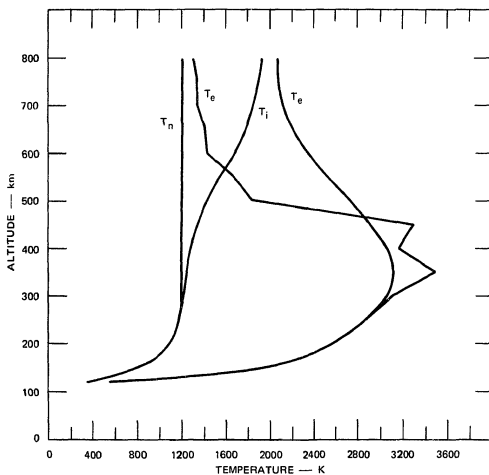
FIGURE 2 ALTITUDE PROFILES OF THE TEMPERATURE FOR THE AURORA AT 1939 AST ON 1 MARCH. Source: Walker and Rees [1968].

Theoretical calculations of ion temperatures in the presence of perpendicular electric fields have been performed by Schunk and Walker [1973] and Rees [1975]. An example of ion temperature as a function of the $\vec{E}$ field magnitude is given in Figure 3. The ion temperature can exceed both the neutral and electron temperatures at ionospheric heights. Temperatures near 3000 K have been predicted as the result of heating by a 60 mV/m orthogonal $\vec{E}$ field. Ion temperatures measured during similar fields are discussed in Section V.

C. Auroral Zone Ion Composition

This dissertation is concerned with the distinction between atomic ions (O^+) and molecular ions (NO^+, O_2^+). (The radar technique does not allow the distinction between NO^+ and O_2^+ to be made, because there is insufficient mass difference between them.) This section will concentrate on the auroral ion chemistry of these ions. The discussion will include what is known both theoretically and experimentally.

Auroral zone ion composition has been studied theoretically by Jones and Rees [1973], Vallance Jones [1974], and others. In addition to the ionization reactions, the principal reactions are as follows:

$$N_2^+ + O \longrightarrow NO^+ + N \qquad (6)$$

$$N_2^+ + O_2 \longrightarrow O_2^+ + N_2 \qquad (7)$$

$$N^+ + O_2 \longrightarrow NO^+ + O \qquad (8)$$

$$N^+ + O_2 \longrightarrow O_2^+ + N \qquad (9)$$

$$O_2^+ + N_2 \longrightarrow NO^+ + NO \qquad (10)$$
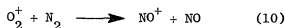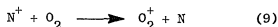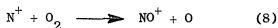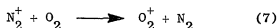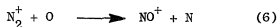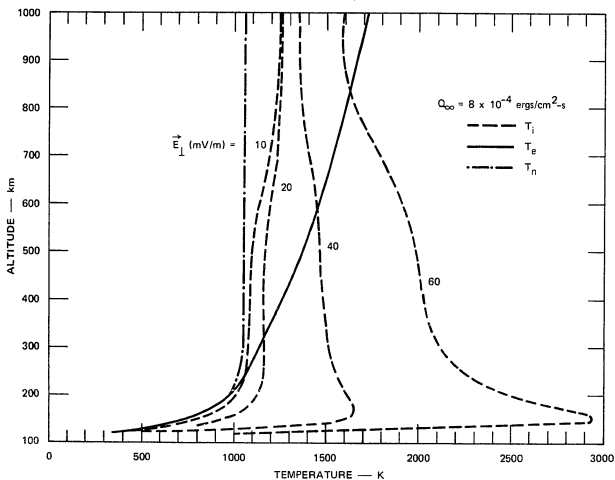
FIGURE 3   ION, ELECTRON, AND NEUTRAL TEMPERATURES RESULTING FROM HEATING BY AN ORTHOGONAL ELECTRIC FIELD. A small magnetospheric heat flux, Q_{∞}, was assumed to exist in the electron gas at 1000 km. For the ion gas $Q_{\infty} = 0$ at the upper boundary. Source: Rees [1975].

$$O_2^+ + N \longrightarrow NO^+ + O \qquad (11)$$

$$O_2^+ + NO \longrightarrow NO^+ + O_2 \qquad (12)$$

$$O^+ + N_2 \longrightarrow NO^+ + N \qquad (13)$$

$$O^+ + O_2 \longrightarrow O_2^+ + O \qquad (14)$$

$$N_2^+ + e \longrightarrow N + N \qquad (15)$$

$$O_2^+ + e \longrightarrow O + O \qquad (16)$$

$$NO^+ + e \longrightarrow N + O. \qquad (17)$$
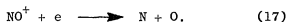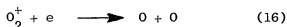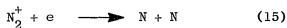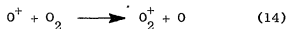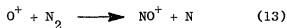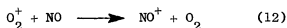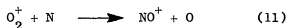
There are also reactions involving excited states--$O^+(^2D, {}^2P)$, $O_2^+(a^4\pi)$-- which produc N_2^+ by

$$O^+ (^2D) + N_2 \longrightarrow N_2^+ + O \qquad (18)$$

$$O^+ (^2P) + N_2 \longrightarrow N_2^+ + O \qquad (19)$$

$$O_2^+ (a^4\pi) + N_2 \longrightarrow N_2^+ + O_2. \qquad (20)$$
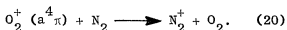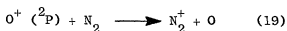
There are, of course, other reactions, however, those listed above are the principal ones.

The reaction-rate coefficients have largely been determined by laboratory measurements; consequently, in principle the coupled continuity equations for the various species can be solved. The results give profiles of the various ion concentrations. The variations of the concentrations of NO^+ and O^+ are particularly important to this study. Figure 4, taken from Jones and Rees [1973], indicates the calculated effect of auroral precipitation on the ratio of the number densities of NO^+ to O^+.
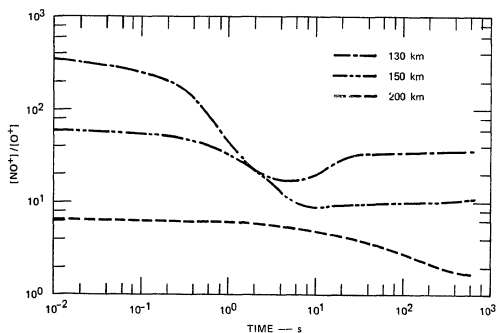
FIGURE 4 TEMPORAL VARIATION OF THE COMPOSITION RATIO [NO$^+$]/[O$^+$]
AT SEVERAL ALTITUDES, DURING BUILDUP OF IONIZATION.
Source: Jones and Rees [1973].

Following the onset of the particle flux, a gradual buildup of O^+ occurs above about 130 km. The O^+ ions are produced by electron impact with O atoms, and NO^+ ions are produced mainly by the reaction involving N_2^+ to O. The lifetimes of NO^+ and O^+ are quite different--the lifetime of O^+ is approximately 20 times that of NO^+ at 130 km; consequently, the ratio $[NO^+]/[O^+]$ * decreases. The ratio at 200 km tends toward unity after onset of the precipitation.

The other molecular ions, O_2^+ and N_2^+, also become more abundant during precipitation. The ions are produced by electron impact and by reactions (6) through (14) and (18) through (20), above. Swider and Narcisi [1974] have measured ion composition with rocket-borne mass spectrometers. Figure 5 indicates their results from data collected over Poker Flat during an intense auroral event (IBC class 3 intensity). It can be seen that at 170 km the concentrations of NO^+ and O^+ are nearly equal. Unfortunately, composition profiles before the auroral event were not measured, so it is not known if the ratio $[NO^+]/[O^+]$ is increasing or decreasing with time. The N_2^+ ion concentration remains insignificant while the O_2^+ concentration is about half that of NO^+.

Schunk et al. [1975, 1976] have investigated the effects of large $\vec{E}$ fields on the concentrations of NO^+ and O^+ at high latitudes. They suggest that during periods of large $\vec{E}$ fields the dominant F-region ion could be NO^+. This could be due to a number of processes:

- enhanced $[N_2]$
- enhanced N_2 vibrational temperatures
- enhanced ion temperatures.

---
* Square brackets indicate number density.
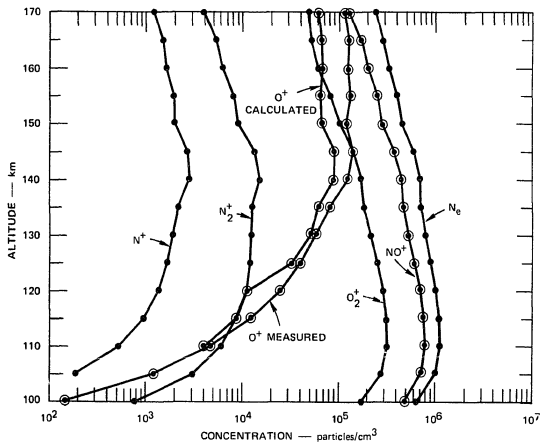
FIGURE 5 CALCULATED N^+, N_2^+, AND O^+ DISTRIBUTIONS AND 27 MARCH 1973 POKER FLAT AURORAL DATA. Source: Swider and Narcisi [1974].

During periods of large energy input through joule heating, it is expected that the neutral atmosphere should be heated by ion-neutral collisions. Hays et al. [1973] have shown that a heated volume element of neutral particles will rise with a vertical velocity which increases with altitude. This expansion will cause an upwelling of N_2 molecules, thereby increasing the number density of N_2 at higher altitudes. The number density of NO^+ will be enhanced because more N_2 is available to either react with O^+ to form NO^+, or be ionized forming N_2^+, which reacts with O forming NO^+.

Another contributing factor to the enhancement of NO^+ ions is the dependence of certain reaction rate coefficients on temperature. The rate coefficient for the reaction $O^+ + N_2 \rightarrow NO^+ + N$ from Banks et al. [1974] is

$$K_1 = \begin{cases} 1.2 \times 10^{-12} \left(\dfrac{300}{T_{eff}} \right) cm^3/s & T_{eff} < 750 \\[3ex] 8.0 \times 10^{-14} \left(\dfrac{T_{eff}}{300} \right)^2 cm^3/s & T_{eff} > 750 \end{cases}$$

where $T_{eff} = T_n + 0.329 \ \vec{E}_\perp'^{\,2}$, and $\vec{E}_\perp'$ is the orthogonal $\vec{E}$-field measured in the neutral-wind frame. This is a simplified form assuming $\nu_i/\Omega_i \ll 1$ and B = 0.5 G (Polar region).

As an example, for an $\vec{E}$ field of 50 mV/m, and T_n = 900 K, T_{eff} will be increased by a factor of 1.9 as compared to T_{eff} for no $\vec{E}$ field. This in turn increases K_1 by a factor of 3.7. The result should be an

enhancement in the number of NO^+ ions. The ions are lost through dissociative recombination. The recombination-rate coefficient decreases with increasing electron temperature [Walls and Dunn, 1974]; consequently, the net result is an increase in the number density of molecular ions.

The third point relative to the production of NO^+ concerns the reaction $O^+ + N_2^* \rightarrow NO^+ + N$, where N_2^* is vibrationally excited N_2. The reaction rates for this reaction are enhanced as compared to $O^+ + N_2$ [Banks et al., 1974]. In the auroral oval, N_2 becomes vibrationally excited through the processes

$$e \text{ (energetic electrons)} + N_2 \rightarrow N_2^* + e \qquad (21)$$

$$N + NO \rightarrow N_2^* + O \qquad (22)$$

$$O(^1D) + N_2 \rightarrow N_2^* + O \ (^3P). \qquad (23)$$
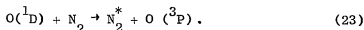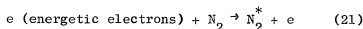
All of these processes could act jointly--i.e., (1) enhanced number density of N_2, (2) enhanced reaction rate coefficients due to elevated T_i, and (3) enhanced reaction coefficients due to vibrational excitation of N_2. The first and second processes are mainly a result of joule heating, and the third process results from electron precipitation.

III   EXPERIMENTAL METHOD

A.   Incoherent-Scatter Theory

As mentioned earlier, the scattering of electromagnetic energy by free electrons in the ionospheric plasma provides a means for the remote probing of the ionosphere. The spectral density function of the back-scattered signal gives a measure of the ionospheric dynamics, thermal structure, and electron density.

Incoherent-scatter theory has been developed by many authors over the last 25 years. The initial theoretical work was performed by Gordon [1958], and it has been advanced by him and others such as Dougherty and Farley [1960], Salpeter [1961], Hagfors [1961], Fejer [1961], and Moorcroft [1963]. The first experimental work was performed by Bowles [1958] when he verified Gordon's theory that incoherent scatter was detectable with radar systems existing at that time. Gordon anticipated that the backscatter spectrum would be quite broad (on the order of MHz) due to the electron thermal motion. Bowles did observe echoes from ionospheric heights; however, the bandwidth was narrower than that predicted by Gordon.

It is now well known that within the ionospheric plasma the electron thermal motions are influenced by the ions. In a thermal plasma, density fluctuations exist due to this ionic influence. The collective interaction between the electrons and ions within a Debye length produces electrical forces that can be visualized as ion waves. These ion

17

waves propagate through the ionosphere at acoustic velocities and are responsible for electron density fluctuations. The incident RF energy will be preferentially scattered by density fluctuations that have a spacing of λ_e, which, according to the Bragg scattering formula is

$$\lambda_e = \frac{\lambda}{2 \sin (\phi/2)}$$

where

λ = Radar wavelength

ϕ = Scattering angle.

For the backscatter case, this expression becomes simply $\lambda/2$.

If the radar wavelength is sufficiently small (less than the distance over which the electrons are influenced by ions--i.e., the Debye length), the electrons can react to the RF wave independently of the ions. In this case, the spectral shape is determined only by the thermal fluctuations of the electrons. The parameter $\alpha^2 = (4\pi D/\lambda)^2$ is used to describe the relationship between λ and the Debye length, D. When λ is small compared to D as in the situation just described, then $\alpha \gg 1$. When $\alpha \ll 1$, the ionic interaction with electrons becomes important and the corresponding spectrum is narrowed and spectral width indicates the ion thermal speed. The width of the spectrum is proportional to the Doppler shift imparted by ions with average speed toward the radar of $\vec{V}_i$, where the spectral width is approximately

$$\Delta f = \vec{V}_i / \lambda_e \ .$$

This simplified picture is complicated when the effects of colli-
sions, the presence of a magnetic field, unequal ion and electron tem-
peratures, and a mixture of ions are included. All of these factors
have an effect on the shape of the backscattered signal spectrum. In
addition, since the Debye length varies with electron density and tempera-
ture, the spectral shape may vary if α does not remain $\ll 1$. When these
factors are taken into account, a complex expression for the frequency
dependence of the incoherent backscatter signal can be derived. In
general terms,

$$S(\omega) = \frac{F_{oi}(\omega/k)}{\left|D(\omega/k)\right|^2}$$

where $F_{oi}(\omega/k)$ is the velocity distribution function for ions and $D(\omega/k)$
is the plasma dispersion relation. The denominator is a minimum at the
ion acoustic frequency, and $S(\omega)$ peaks at that frequency. The resulting
spectral shape then has the characteristic ion line peaks (see Figure 6).

B. Previous Temperature and Composition Studies Using

    Incoherent-Scatter Radar

Measurements of ionospheric temperatures and composition have been
performed with midlatitude incoherent-scatter radars by a number of
authors [Evans and Cox, 1970; Wand, 1970; Waldteufel, 1971; Evans and
Oliver, 1972; and Alcayde et al., 1974]. The techniques used to deter-
mine the composition differ somewhat according to the capabilities of
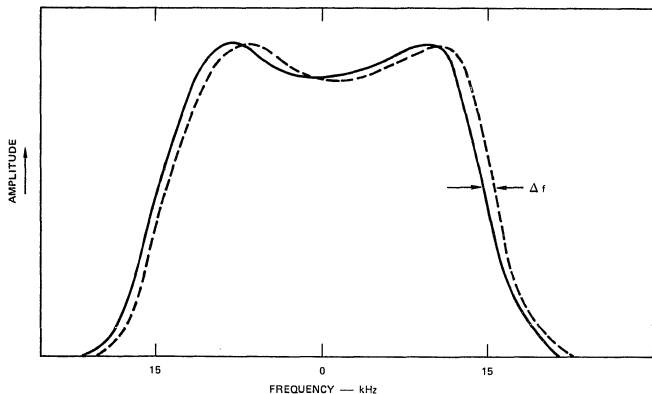
FIGURE 6   INCOHERENT SCATTER SPECTRAL SHAPE. The shape of the spectrum is a function of the electron to ion temperature ratio and of the ion temperature to ion mass ratio. Also indicated is the Doppler effect (Δf) produced by an ion velocity.

the radar used. Two basic techniques, which will be described, were used at the Arecibo Observatory and with the Millstone and St. Santin systems.

The temperature and composition data are contained in the shape of the spectrum from the ionic component of the backscattered signal. However, T_i, T_e, and ion composition cannot be uniquely determined, since it is the ratios, T_e/T_i (T_r) and T_i/M_i that determine the spectral shape We have two parameters containing three unknowns. Either assumptions must be made, or an independent measurement of one of the three unknowns is required in order to determine the other two.

The experiments performed by Wand [1970] at Arecibo used a technique that employed two independent measurements of N_e. The first determination of N_e used the returned signal from the plasma line. The frequency shift of the plasma line is proportional to N_e. The second determination of N_e used the power received from the ion line component. The received power is proportional to both N_e and the temperature ratio. Therefore by comparing electron densities determined from the plasma frequency (plasma line observation) with densities determined from power measurements from the ion component, the temperature ratio can be determined. The temperature ratio is related to composition by the function B (q); $T_r(q) = B(q)T_r(1)$ [Wickwar, 1974] where $q = [O^+]/\{[O^+] + [NO^+] + [O_2^+]\}$, and $T_r(1)$ is the temperature ratio assuming entirely O^+. The function B(q) is shown in Figure 7.
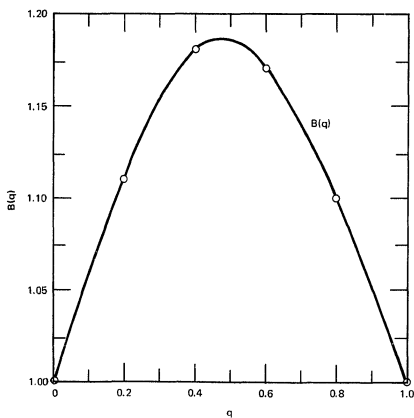
FIGURE 7   VALUES OF B(q) AS A FUNCTION OF q. Source: Wickwar [1974].

The more serious limitations of this method are the following:

(1) T_r varies less than 20% as a function of composition and consequently is insensitive to q. If one were to compute q as a function of altitude, the altitude where q = 0.5 could be in error as much as ± 25 km. (2) The electron density measurements at Arecibo require a correction for antenna near-field effects.

The alternative method for computing composition requires that either an initial estimate of the composition profile or an estimate of the T_i profile be made. If a model of the altitude dependence of q is obtained--from rocket data, for instance [Carru et al., 1967], then from the measured spectra, T_i and T_e profiles can be determined. The q profile is then varied ± 10% and two new profiles for T_i and T_e are determined. Smooth curves are drawn through T_i and T_e points such that they connect to the upper and lower values where composition is known (130 km NO^+ and 240 km O^+). Thus, a new q profile is determined.

The other method requiring an assumption relies on the hypothesis that $T_i = T_n$ in the altitude region below about 250 km. A T_n profile can be determined by measuring T_i where the composition must be O^+. Evans uses the mean ion temperature taken at 229, 261, and 294 km as the exospheric temperature. The CIRA 1965 model atmosphere then provides the T_n profile (or, equivalently, the T_i profile). Finally, the composition profile is determined from the function A(q) [Wickwar, 1974], which relates the ion temperature based on entirely O^+ to the ion temperature based on q at a specific height:

$$T_i(q) = A(q) T_i(1) \quad .$$

The function A(q) is shown in Figure 8.

There are certainly limitations to both of these assumption methods. The first method, assuming q profiles, constrains the answer to be close to the initial assumption. The second method requires the use of models because the assumption $T_i = T_n$ is made from the spectral data.

Seasonal and diurnal variations in the relative abundance of O^+ ions have been measured at Arecibo, Millstone, and St. Santin. Generally the results indicate that the transition altitude (q = 0.5) is lower in the winter than in the summer, the largest difference being 60 km, measured at Arecibo. The transition altitude is a convenient parameter to discuss because temporal variations are easily displayed. It is also an indication of the variations of $[O]/[N_2]$ which will be discussed later. The diurnal variations show that the transition altitude decreases with decreasing solar zenith angle (SZA). The variation is on the order of 10 to 15 km.

C.   Technique Used at Chatanika

    1.   General

        The determination of composition results from an analysis of ion temperature profiles or in some cases electron temperature profiles. The entire process is indicated in the flowchart in Figure 9.

        The starting point is the determination of the autocorrelation functions of the backscattered signals. This is done with a digital autocorrelator in real time--the resulting ACFs are integrated (typically
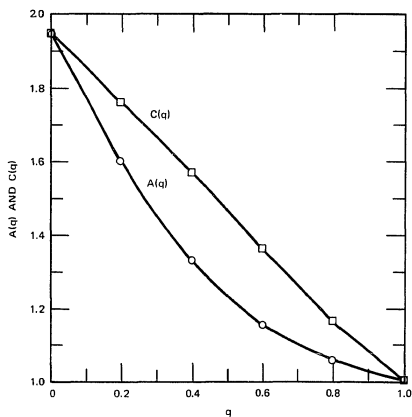
FIGURE 8 VALUES OF A(q), AND C(q). Source: Wickwar [1974].

MEASURED ACFs

↓

ESTIMATE T_r', T_i
(zero crossing + 1st minimum)

↓

FIND THEORETICAL ACF
FOR ABOVE T_r' AND T_i

↓

UPDATE ESTIMATE OF T_r' AND T_i
BY LEAST SQUARES FIT

↓

DEBYE CORRECTION TO
OBTAIN T_r AND N_e

↓

ASSUME 100% O^+

↓

OUTPUT
T_r, T_i, N_e

↓

$\vec{J} \cdot \vec{E}'$ > 5 ergs/cm²-s

NO →

ASSUME
$T_i(h) = T_N(h)$

↓

TAKE T_N PROFILE
FROM CIRA 72
FOR $T_N(250) = T_i(250)$

↓

ADJUST COMPOSITION
SO THAT $T_i = T_N$ AT ALL
ALTITUDES BELOW 250 km

↓

OUTPUT
COMPOSITION vs. ALTITUDE

YES →

αN_e^2 > 5 ergs/cm²-s

NO →

PLOT
T_e vs. TIME

↓

APPARENT
T_e DECREASE

↓

SET
$T_e(h) = T_e(h)$ BEFORE HEATING
BY ADJUSTING COMPOSITION

↓

OUTPUT
COMPOSITION vs. ALTITUDE

YES →

Same procedure
as NO. However,
only a lower
bound is
determined.

FIGURE 9   FLOWCHART DESCRIBING THE ALGORITHM USED TO DETERMINE ION
COMPOSITION. Two techniques are used depending on the magnitude of
joule heat input. (5 ergs/cm²-s would enhance the ion temperature about
100 k--which is on the order of the largest error bars expected.)

15 s) and are recorded on magnetic tape. A computer program (MITFIT) is used to perform a least-squares fit of these measured ACFs to a library of theoretical ACFs.

The theoretical autocorrelation functions are computed using the equation from Fejer [1961] for frequency dependence of the back-scattered signal about the transmitted frequency:

$$S(\omega) = \frac{\left| 1 + \sum_{j=2}^{N} F_j \right|^2 \left(\frac{1}{\Omega_1} e^{-\omega^2/\Omega_1^2} \right) + \left| F_1 \right|^2 \left(\sum_{j=2}^{N} \frac{f_j}{\Omega_j} e^{-\omega^2/\Omega_j^2} \right)}{\left| 1 + \sum_{j=1}^{N} F_j \right|^2}$$

where

$f_j \equiv N_j/N_1$, the fractional concentration of the jth ion

$\Omega_j \equiv \frac{4\pi}{\lambda} \sqrt{\frac{2k\,T_j}{m_j}}$

λ = Radar wavelength

k = Boltzmann's constant

$F_j \equiv \frac{1}{\alpha_j^2} (1 - I)$

$I \equiv i\omega \int_0^{\infty} \exp\left(-i\omega t - \frac{\Omega_j^2 t^2}{4} \right) dt$

$\alpha_j^2 \equiv \left(\frac{4\pi D_j}{\lambda} \right)^2$

$$D_j^2 \equiv \frac{\varepsilon_o \; kT_j}{e^2 N_j} \quad \text{(in mks units, } \varepsilon_o \text{ is the permittivity of free space)}$$

$$\equiv \frac{k \; T_j}{4\pi \; e^2 \; N_j} \; , \text{ the Debye length squared (in esu)}.$$

This equation is used to calculate the theoretical spectra. In turn, the theoretical autocorrelation functions (ACFs) for the incoherent-backscatter signal were obtained by Fourier transforming the spectra using the FFT routine by Singleton [1969].

The fitting process uses an initial value of the temperature ratio (T_r') and the value of T_i from the zero crossing and first minimum of the ACF. The program then performs a least-squares fit for all of the autocorrelation coefficients until the following function is minimized:

$$\chi^2 = \sum_{n=1}^{\ell} \left[\frac{(\text{Lib ACF}_n - \text{X ACF}_n)^2}{\sigma_n^2} \right]$$

where

ℓ = Number of lags

Lib ACF = Theoretical autocorrelation function

X ACF = Measured autocorrelation function

σ_n^2 = Variance for each lag of X ACF

The Lib ACFs are computed for 100% O^+ ions. Then the raw density, N_e', is corrected for the Debye length and the electron to ion temperature

ratio by an iterative process [Baron et al., 1970]. The final values are related to the initial values by the following equations

$$T_r = (1 + \alpha^2)T_r'$$

$$N_e = \frac{(1 + \alpha^2 + T_r)(1 + \alpha^2)}{2} N_e'$$

$$\alpha^2 = (4\pi D_e/\lambda)^2$$

where

$$T_r = T_e/T_i$$
$$D_e = \text{Debye length}$$

The final values are found by iterating upon the equations for α^2 and N_e holding T_r constant.

At this point, the data concerning the ion velocity and hence the perpendicular electric fields are examined. The joule heating, $\vec{J} \cdot \vec{E}$, (where $\vec{E}$ is the electric field in the neutral wind frame) is computed.

2. Case 1 - No Joule Heat Input

If no significant joule heating occurred (< 5 ergs/cm^2-s), which would cause a temperature difference $T_i - T_n \approx 100$ K, then the assumption is made that the ions should be in thermal equilibrium with the neutrals. Next, a neutral temperature profile is chosen from the CIRA 1972 model ionosphere. The particular profile is chosen by using an ion temperature (equivalent to the neutral temperature), measured at an altitude where the assumption of 100% O$^+$ is most probably valid-- generally 250 km. Therefore, the CIRA 1972 profile that satisfies the

measured temperature at 250 km is used. This profile is then compared to the T_i (100% O^+) profile.

At some point below 250 km the assumption of 100% O^+ ions will fail. This is apparent in the comparison of $T_i(h)$ with $T_n(h)$, since T_i begins to fall below the T_n curve. An example of this comparison is shown in Figure 10. At low enough altitudes, T_i (100% O^+) becomes nearly half of the value of T_n, indicating 100% molecular ions. The correction required to equate T_i with T_n indicates the relative abundance of molecular as compared with atomic ions.

3.   <u>Case 2 - Joule Heat Input</u>

During periods of joule heating the assumption that $T_i(h) = T_n(h)$ will not necessarily be valid. Consequently, we use an alternative procedure. We plot T_e versus time for F_1 and F_2 region altitudes and examine these data during the joule heating input period. If a composition change occurred, the electron temperature will appear to decrease because of the assumption of O^+ ions in the least-squares fitting code.

The rate at which electrons cool by collisions with neutrals is

$$\frac{dU}{dt} = - (3m_e/m_n) N_e k \nu_{en} [T_e - T_n] \quad .$$

This cooling rate should remain fairly constant unless the electron density is enhanced. Therefore, a change in apparent electron temperature without an accompanying enhancement in electron density
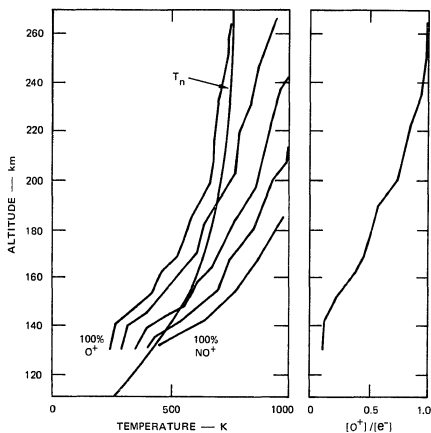
FIGURE 10   ION TEMPERATURES FOR VARIOUS PERCENTAGES OF
O⁺ IONS, AND RESULTING COMPOSITION PROFILE.
The curve, T_n, is the neutral temperature profile from CIRA
1972, corresponding to the 100% O⁺ ion temperature at
260 km.

indicates that the composition has changed such that more molecular
ions are present at the particular altitude. We then alter the compo-
sition so that the apparent electron temperature remains constant
throughout the joule heating period.

It is certainly possible that the electron temperature is
enhanced during the period of joule heating, either from particle pre-
cipitation or from ions when $T_i > T_e$. However, by requiring that the
temperature at least remain constant, a lower limit on the composition
change is determined.

D. Examples of the Effect of Temperature Ratio and Composition
on Spectra and Autocorrelation Functions

Figures 11(a) through 13(a) give examples of spectra. (The spectra
are assumed to be symmetrical; consequently only half of each spectrum
is shown.) Figures 11(b) through 13(b) give corresponding examples of
ACFs for the frequency of the Chatanika radar (1290 MHz) and for a 10-μs
interval between ACF samples. These figures are taken from Wickwar [1974].

Figure 11 shows the effect of varying T_r, or, alternatively, of
varying the electron temperature, T_e. In the ACF, the relative minima
and maxima are seen to be strong functions of T_r. The correlation time
(i.e., time of the first zero crossing) is seen to decrease with increas-
ing electron temperature. Figure 12 shows the effect of varying T_i and
T_e such that T_r is constant. It is seen that the relative minima and
maxima are constant in magnitude, although they occur at different times.
The ACF is further seen to move in and out along the time axis according
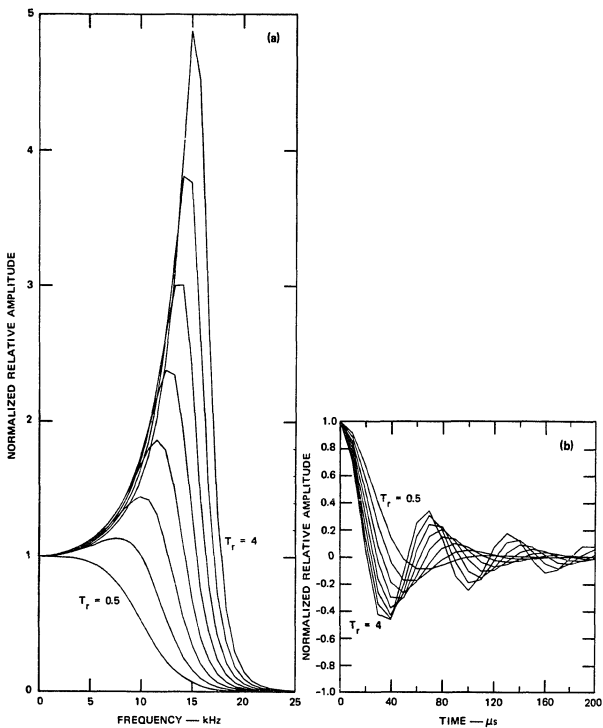
FIGURE 11 T_r VARIATION OF THE POWER SPECTRA AND AUTOCORRELATION FUNCTIONS (ACFs).   The curves show variations in T_r from 0.5 to 4.0 in steps of 0.5 for $T_i = 800°K$, $\alpha^2 \ll 1$, and O^+ composition.
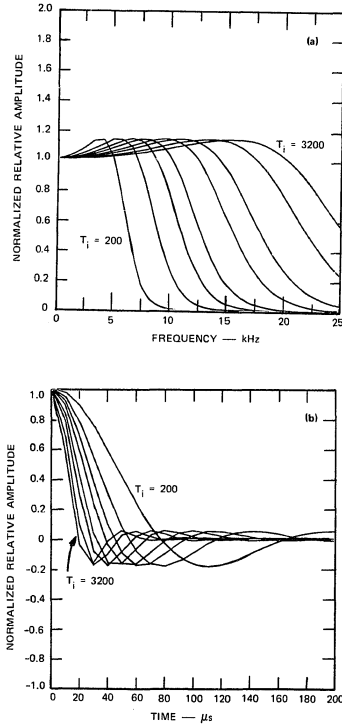
FIGURE 12   THE T_i VARIATION OF THE POWER SPECTRA
AND ACFs. These curves show eight values of
T_i (200, 400, 600, 800, 1200, 1600, 2400, and
3200 K) for T_r = 1.0, $\alpha^2 \ll 1$, and O^+
composition.
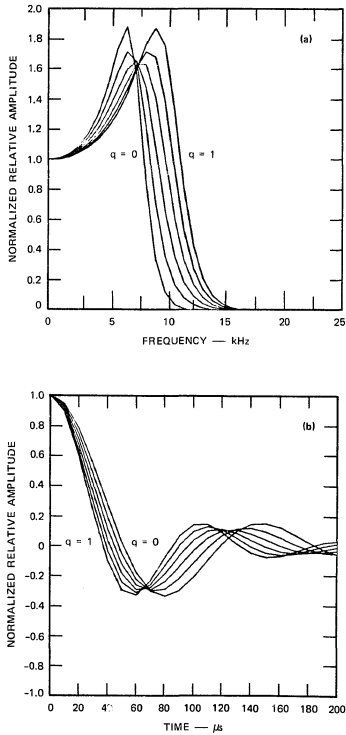
FIGURE 13   COMPOSITION VARIATION OF THE POWER SPECTRA
AND ACFs.   These curves show variations in composition
from entirely mass 31 ions to entirely O^+ ions (from
$q = 0.0$ to $q = 1.0$ in steps of 0.2) for $T_i = 500$,
$T_r = 2.0$, and $\alpha^2 \ll 1$.   Source: Wickwar [1974].

to $1/\sqrt{T_i}$ for a fixed T_r. Figure 13 shows the effect of q. In going from q = 1.0 to q = 0.0 (from O^+ to mass 31.5 ions), the ACF appears to have contracted as though the ion temperature had nearly doubled.

This dependence of the ACF zero crossing on the parameters q and T_i enables us to estimate the composition profiles, if T_i is known or can be estimated. Generally, T_i is estimated from neutral atmospheric models because the ions and neutrals are at the same temperature in the altitude range of this study.

E. The Experiment

The geomagnetic coordinates of the Chatanika incoherent-scatter radar are given in Table 1, and its parameters are given in Table 2.

Table 1

GEOMAGNETIC COORDINATES OF THE CHATANIKA INCOHERENT-SCATTER RADAR

Geographic Coordinates		Dipole Geomagnetic Coordinates		Magnetic Field	
Latitude	Longitude	Latitude	Longitude	Dip Angle	Declination
65.103°N	147.451°W	64.75°N	105.0°W	76.5°	29.0°

The geometrical relationship between Chatanika and the auroral oval for moderate geomagnetic activity is shown in Figure 14. The oval is usually far north of Chatanika at local noon and is often overhead near midnight. The circle (arbitrarily located at 1500 UT) indicates the E-region coverage typical for these experiments.
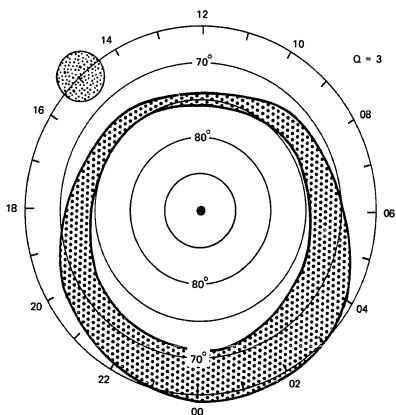
FIGURE 14   CHATANIKA LOCATION (65°N) AND FELDSTEIN'S 1967
AURORAL OVAL. Source: Feldstein and Starkov [1967].

Table 2

PARAMETERS OF THE CHATANIKA INCOHERENT-SCATTER RADAR

Operating frequency	1290 MHz
Transmitted peak power	3 to 4 MW
Pulsewidths	60 μs, 160 μs, 320 μs
Effective antenna aperture	180 m^2
Antenna on-axis gain	47.1 dB
Antenna 1/2-power-full-width beamwidth	0.6°
Transmit polarization	Right circular
Receive polarization	Left circular
System noise temperature	110 K
A/D converter sample spacing	10 μs
On-line computer system	XDS 930

For two of the 24-hour experiments, a pair of 160-μs transmitted pulses were used. The received signal following each backscattered pulse was sampled, and autocorrelation functions were measured by taking lagged products of the appropriate samples. This sampling is repeated 16 times, providing 16 range gates typically placed between 110 and 300 km with a spacing of 12 km. Electron densities are measured with a 67-μs pulse (10 km). The density samples are taken at 10-μs intervals between about 80 km to over 800 km, and are subintegrated three times. The two other 24-hour experiments use a 320-μs pulse for the spectral data. The experimental details are summarized in Table 3.

Table 3

EXPERIMENT PARAMETERS

Date	Pulse Sequence (μs)	Antenna Positions (degrees)	
		Az	El
13 Aug 1975	67 + 320	Scan	65
15 Oct 1975	67 + 320	209*	76.5*
		89	70
		150	70
18 Feb 1976	160 + 160	029	65
		268†	65
		151†	65
13 May 1976	160 + 160	029	65
		260	65
		151	65

Data were collected on the designated international world day of each month beginning in August 1975 and continuing until May 1976. The radar was operated for 24-hour periods, providing electron density, ion velocity, electron and ion temperatures, and ionic composition. The antenna was cycled through three antenna positions, remaining in each position for 5 minutes. The three antenna positions were chosen so that the perpendicular electric field could be resolved from the line-of-sight ion velocity.

*This position is parallel to $\vec{B}$.

†This position is in the L-shell.

The two experiments using the long pulses for spectral data are limited in that the 48-km pulse cannot be used for E-region temperatures or composition analysis because the pulse length is large compared to the scale height. Analysis was not attempted using range gates below 160 km.

The other experiments, which use the shorter 160-μs (24 km) pulses, suffer from a different problem. In order to maintain the same range capability, the same pulse repetition frequency is used; consequently, the shorter pulses contain less power in a given time interval. As a result, the signal-to-noise ratio (SNR) is poor, especially at altitudes above 200 km. During the night portion of these experiments it was often impossible to obtain reliable temperatures.

F.   Derivation of Other Parameters

Other parameters that are derived from radar measurements include $\vec{V}_i$, $\vec{E}_\perp$, joule heat input, and particle energy deposition. The method used to resolve the ion velocity from the line-of-sight velocities and $\vec{E}_\perp$ are documented in Rino [1972]. The joule heating computations are documented in Brekke and Rino [1978], and the particle energy deposition calculations are found in Wickwar et al. [1975].

Briefly, the resolved ion velocities are obtained from a sequence of measurements made with the antenna pointed in three different directions. The most common case uses three different azimuths at one elevation angle. The vector ion velocity ($\vec{V}_i$) is then determined from the three line-of-sight velocity measurements.

The ion equation of motion provides the relation between the ion velocity and the electric field:

$$M_i \left(\frac{\partial \vec{V}}{\partial t}\right) = q(\vec{E} + \vec{V}_i \times \vec{B}) + M_n \, \nu_{in}(\vec{U} - \vec{V}_i) \qquad .$$

where

      M_i = Ion mass

      q = Electron charge

      $\vec{E}$ = Electric Field

      $\vec{V}_i$ = Ion velocity

      $\vec{B}$ = Magnetic field intensity

      M_n = Neutral mass

      ν_{in} = Ion-neutral collision frequency

      $\vec{U}$ = Neutral velocity.

This equation reduces to

$$\vec{E}_\perp = \vec{V} \times \vec{B}$$

because the relatively long integration times of 5 minutes allow steady-state conditions ($\partial \vec{V}/\partial t = 0$) to be assumed, and because at altitudes above 150 km, ν_{in} is small.

Joule heat input is computed from the relation

$$Q = N_e \, \nu_{in} \, M_i \, (\vec{V}_\perp - \vec{U}_\perp)^2 \qquad .$$

The E-region neutral wind is given by

$$\vec{U}_\perp = \vec{V}_i - \frac{\Omega_i}{\nu_{in}} (\vec{E}_\perp + \vec{V} \times \vec{B})$$

where

$\nu_{in} = CN$

$C = 3.75 \times 10^{10} cm^3/s$ (C is the rate coefficient, i.e.,

rate of momentum transfer per unit volume)

N = Neutral number density from 1000 K atmosphere in

Banks and Kockarts [1973].

The particle energy deposition is found from the equilibrium

relation

$$Q_p = \alpha_{eff}(h) N_e^2$$

where

$\alpha_{eff}(h)$ = Height-dependent effective recombination coefficient

[Wickwar et al., 1975]

N_e = Measured electron density

The particle energy is then computed from the production rate Q,

assuming 35 ev are liberated per ion pair produced.

IV   DATA

The radar data were reduced using the techniques and computer programs described in the previous section. Before presenting the data from the continuous 24-hour periods, we first show a comparison between radar-measured composition profiles and a rocket-measured profile taken at the same time.

A.   Verification of Technique--University of Texas at Dallas Rocket Comparison

On 28 February 1976, a Nike Tomahawk rocket carrying a University of Texas at Dallas (UTD) payload was launched from Poker Flat. The payload instrumentation included probes for measuring ion and electron densities and a positive-ion mass spectrometer. The radar was operated before, during, and after the flight in order to obtain background as well as simultaneous data. The data that will be compared directly are the ion composition profiles.

This night was moderately active, as indicated by the College, Alaska magnetometer traces in Figure 15. The launch occurred at 1213 UT and the radar was operated from about 1000 UT to 1300 UT. The measured $\vec{E}$-fields are shown in Figure 16. The north-south component was directed to the south and was also relatively small (< 20 mV/m). The resulting height-integrated joule heating is plotted in Figure 17. The heat input is 3 ergs/cm^2-s or less, prior to and during the flight. This input is small, and consequently the ion temperatures were not significantly enhanced (< 100 K). The energy deposition from precipitation is

43

FIGURE 15   MAGNETOGRAM FOR 28 FEBRUARY 1976
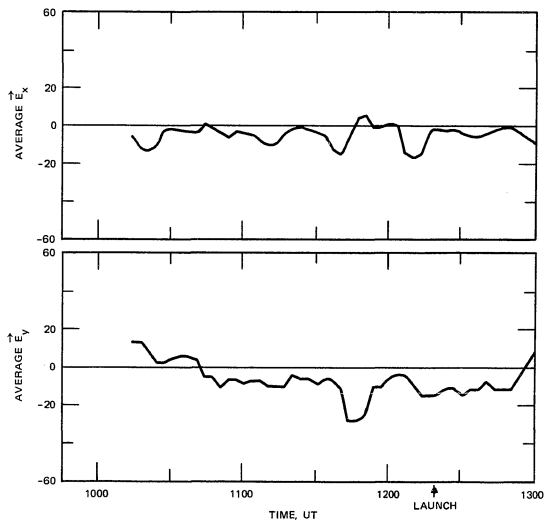
FIGURE 16 AVERAGE ELECTRIC FIELD FOR 28 FEBRUARY 1976. E_x is positive to the East; E_y is positive to the North.
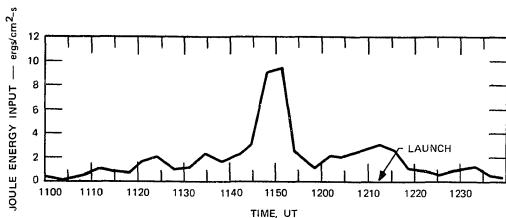
FIGURE 17   HEIGHT-INTEGRATED JOULE HEATING FOR 28 FEBRUARY 1976
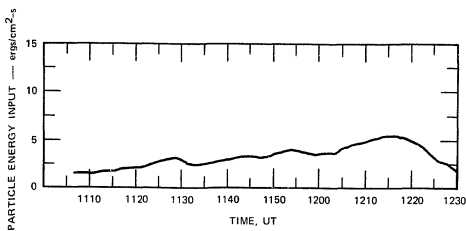
FIGURE 18   PARTICLE ENERGY INPUT FOR 28 FEBRUARY 1976

shown in Figure 18 and is on the order of 5 ergs/cm^2-s. This small input represents an average over a 5 minute period.

The radar beam was pointed along the rocket up-leg trajectory from 1215 to 1219 UT. The electron density profile measured during that period agrees quite well with the profile measured by the rocket. The ion temperature data were integrated during those five minutes, and are indicated in Figure 19. Six ion temperature profiles are shown, each corresponding to a different assumed $[O^+]/N_e$ ratio. Also shown is the neutral temperature profile from the CIRA 1972 model for an exospheric temperature of 900 K. This exospheric temperature was chosen based on ion temperatures at altitudes above 210 km, where O^+ ions should dominate the composition.

The composition in the transition region is then indicated by the intersection of T_n with the parameterized T_i profiles. The resulting composition profile is shown in Figure 20. Also shown is the composition profile resulting if a different model atmosphere is used [Banks and Kockarts, 1973], and the profile inferred from the rocket data. All three curves are in good agreement, indicating that the technique is not particularly sensitive to the assumed model atmosphere. The CIRA 1972 model was used for the remainder of the analysis.

B. 24-Hour Experiments

For each of the 24-hour periods the electron and ion temperatures were determined. The temperatures presented here are from range gates at altitudes where O^+ ions usually dominate (generally above 220 km).
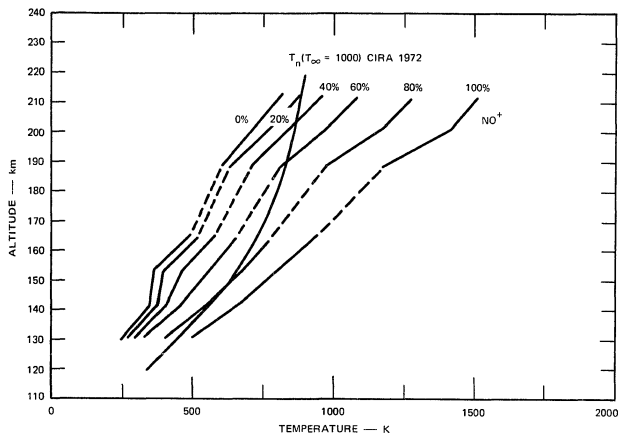
FIGURE 19   ION TEMPERATURES PARAMETERIZED BY COMPOSITION FOR 28 FEBRUARY 1976
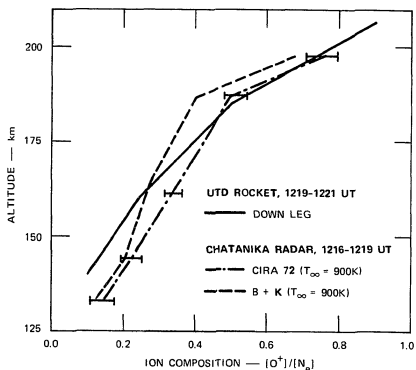
FIGURE 20 COMPARISON OF COMPOSITION PROFILES FROM ROCKET DATA AND RADAR DATA USING TWO DIFFERENT MODELS--28 FEBRUARY 1976

The perpendicular electric field is also computed for the entire period. Where the electric field is significant (> 10 mV/m) the joule heating is computed. This indicates periods when the ion temperatures are expected to be enhanced, and consequently the assumption $T_i = T_n$ will not be used. The energy deposition from precipitating auroral electrons is also computed. Finally, the ion composition is given in terms of contours of q, where q = $[O^+]/N_e$, generally between 160-220 km. Error bars are shown for temperature and composition data and are discussed in the Appendix.

1. 13 May 1976

The quietest 24-hour period analyzed was 13 May 1976. The magnetometer traces for the period are indicated in Figure 21. As a result of the quiet conditions, the SNR was low whenever the SZA exceeded about 103°. This results in rather large error bars for most of the derived parameters. Data from 0800 to about 1400 UT are consequently ignored.

The perpendicular electric fields are shown in Figure 22. As can be seen, both the north-south and the east-west electric fields are small; the resulting joule heating was computed and found to be less than the threshold value of 5 $ergs/cm^2$-s.

During the early morning there was a small amount of particle precipitation. A plot of the resulting energy deposition is shown in Figure 23. The height-integrated energy input was less than 3 $ergs/cm^2$-s. The smooth curve is the decay and growth of the ionization in the E layer produced by the solar extreme ultraviolet (EUV) radiation. The apparent
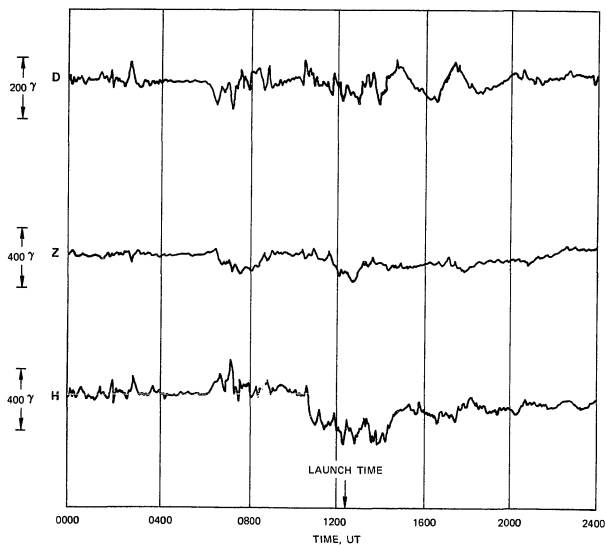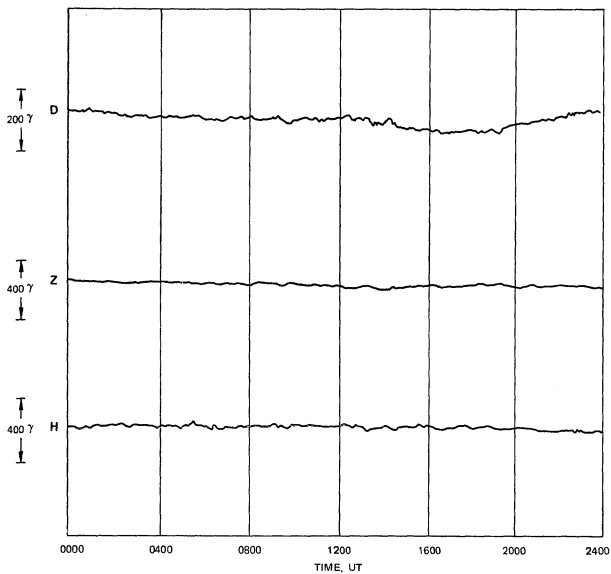
FIGURE 21   MAGNETOGRAM FOR 13 MAY 1976

FIGURE 22 AVERAGE ELECTRIC FIELD FOR 13 MAY 1976. E_x is positive to the East; E_y is positive to the North.
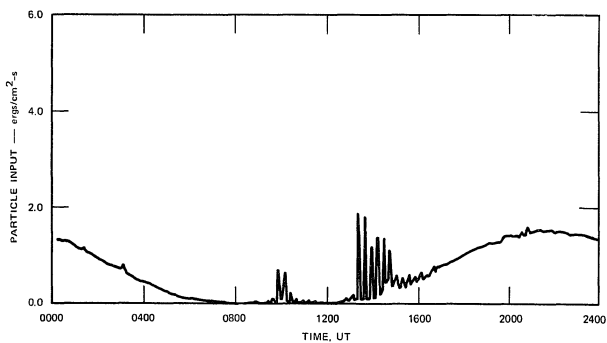
FIGURE 23   PARTICLE ENERGY DEPOSITION FOR 13 MAY 1976

periodic structure is an artifact of cycling through three antenna positions, and therefore reflects spatial inhomogeneities.

The F-region temperatures are indicated in Figure 24. The 24-hour runs begin at 0000 UT, which is 1400 local time. Consequently the F region is sunlit and the temperatures should be maximum near 0000 UT. The minimum should occur near 1000 UT, when the SZA is maximum. The electron temperatures do tend to decrease after 0600 UT; however, the SNR is insufficient to determine reliable temperatures between 0800 and 1400 UT. The electron temperatures vary between 2200 K and 1000 K from 0000 UT to 1400 UT. The variation in the ion temperatures is much less, and differs from model predictions. The maximum temperature would be expected near 0200 UT, corresponding to minimum SZA. This is predicted by the Jacchia 1971 Model and is discussed in Section V.

The composition contours are shown in Figure 25 They indicate that the transition altitude did not change appreciably during the 24 hours. The only noticeable change is in the thickness of the transition region. The thickness measured from q = 0.4 to q = 0.8 is about 35 km in the afternoon (0000 UT) as compared to 20 km at 1900 UT.

2.   15 October 1975

15 October 1975 was somewhat more active than the 13 May example; however, the activity was only moderate. In addition, since it is close to the autumnal equinox, diurnal variations are more apparent. The degree of activity can be seen in the College, Alaska magnetometer traces shown in Figure 26. The only significant feature occurs between 1100 and 1200 UT.
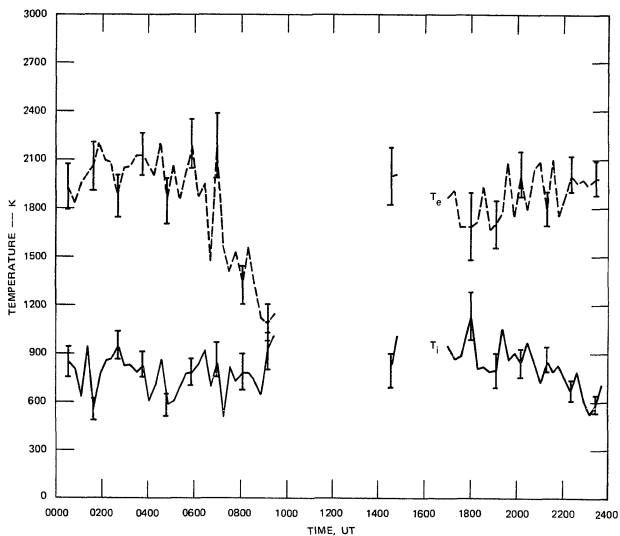
FIGURE 24   ELECTRON AND ION TEMPERATURE AT 232 km FOR 13 MAY 1976
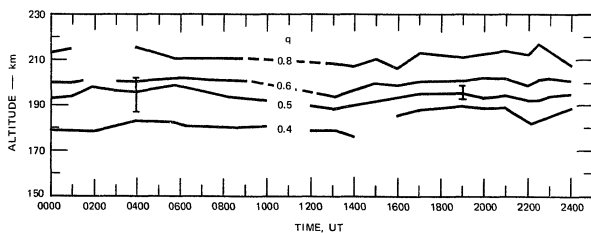
FIGURE 25   ION COMPOSITION CONTOURS FOR 13 MAY 1976--CONTOURS OF $q(q = [O^+]/N_e)$
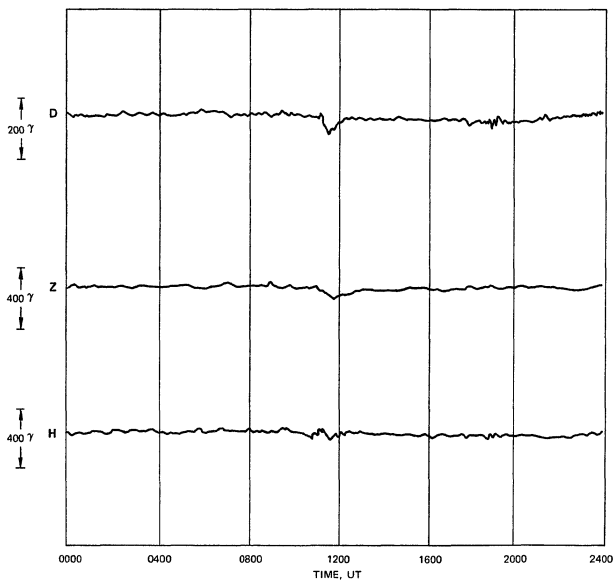
FIGURE 26   MAGNETOGRAM FOR 15 OCTOBER 1975

The electric fields were again small throughout most of the 24-hour period. (The data are shown in Figure 27.) During the night portion of the run, 0500 to 1000 UT, the SNR was small, causing the electric field data to be noisy. However, it can be seen that no significant $\vec{E}$-fields existed after 0700 UT; consequently, no significant joule heating occurred.

There was, however, particle precipitation beginning near midnight. The energy deposition due to this precipitation is plotted in Figure 28. The peak deposition occurred at 1130 UT at about 20 ergs/ cm^2-s. This was responsible for the elevated electron temperature during that period.

Figure 29 indicates the electron and ion temperatures at 218 km. The temperature variations are much greater on this day than on 13 May 1976. This is primarily due to the much greater variation in SZA. At night, when the SZA is $> 104^{\circ}$, the electron temperature at 218 km is about 600 K while after sunrise the temperature increases to almost 1600 K at that altitude. The ion temperature also shows some increase in exospheric temperature with changing SZA. In addition, around 1200 UT the effect of precipitation can be seen as the electron temperature increases nearly 400 K.

The composition contours for 15 October 1975 are shown in Figure 30. The contours indicate that as the SZA decreases, the transition altitude also decreases. Nighttime transition altitudes are between 180 and 190 km; during the day the altitude is between 170 and 180 km.
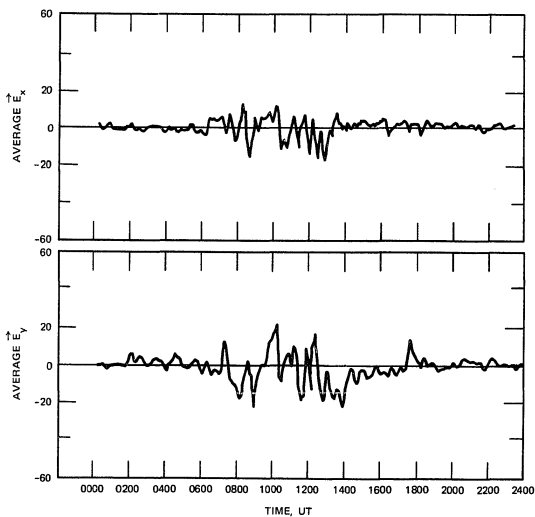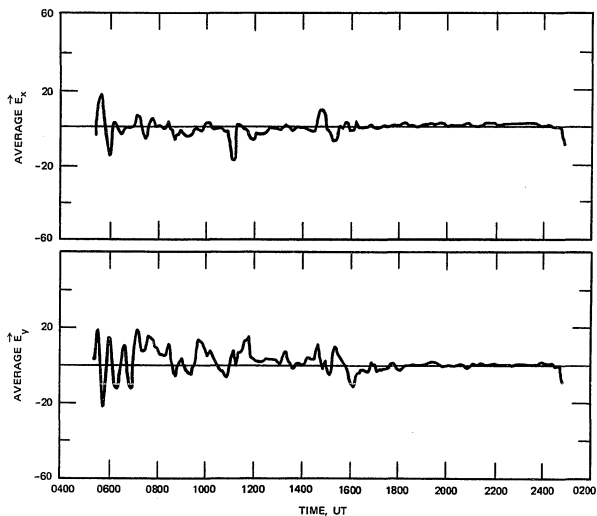
FIGURE 27   AVERAGE ELECTRIC FIELD FOR 15 OCTOBER 1975. E_x is positive to the East; E_y is positive to the North.
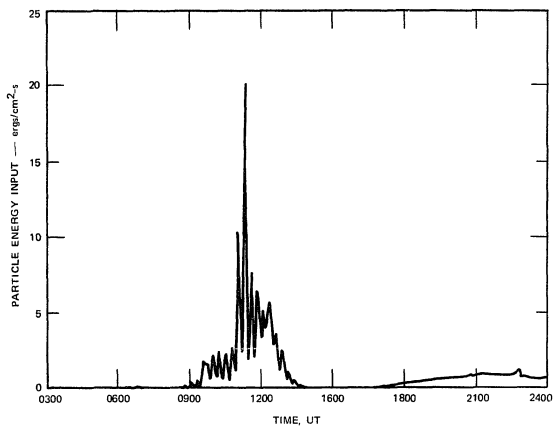
FIGURE 28   PARTICLE ENERGY INPUT FOR 15 OCTOBER 1975
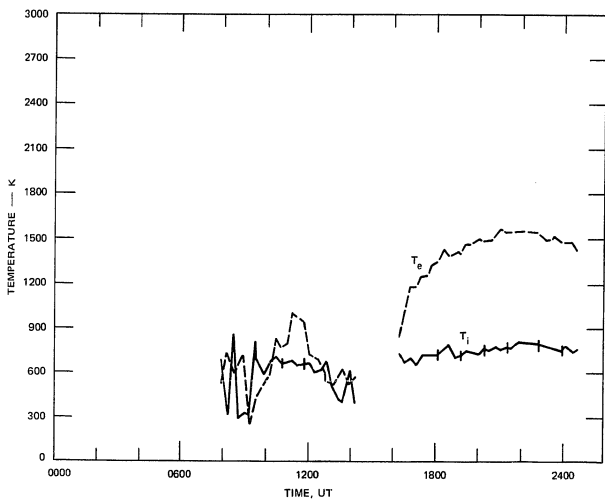
FIGURE 29 ELECTRON AND ION TEMPERATURE AT 218 km FOR 15 OCTOBER 1975
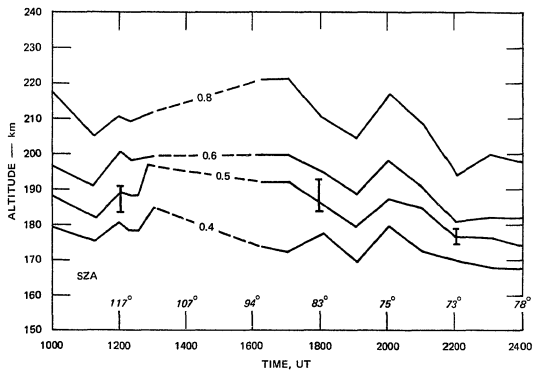
FIGURE 30   ION COMPOSITION CONTOURS FOR 15 OCTOBER 1975

3. <u>13 August 1975</u>

13 August 1975 was characterized by a moderate magnetic disturbance. The magnetogram is displayed in Figure 31. The period between 0800 to 1600 UT is especially disturbed.

The electric field was computed for the 24-hour period and it shows the characteristic daily variation pattern of auroral zone electric fields. The north-south field is plotted in Figure 32. In the evening prior to local midnight, the field is directed to the north. Near midnight the field reverses and is directed south during the early morning. The field becomes quite large at 1400 UT--nearly 60 mV/m. The resulting joule heating is plotted in Figure 33. At 1400 UT the energy input is about 30 ergs/cm^2-s which is substantial. This is the largest joule heating event analyzed in this limited data base, and, as will be seen, its effects are considerable.

The electron and ion temperatures at 276 km are shown in Figure 34. At the start of the run, 0000 UT, the ion temperature is fairly constant with a value of 900 K. There is little change in the temperature until about 1000 UT, when the joule effect begins. There is an obvious enhancement in ion temperature at 1400 UT--the peak of the joule input. The temperature remains elevated even after the joule heat source terminates at 1500 UT, being about 100 K higher than the earlier temperatures. The temperature gradually decreases and it returns to initial conditions by 2300 UT.

The electron temperature shows the effect of the changing SZA. Initially, the temperature is about 2200 K and it gradually decreases
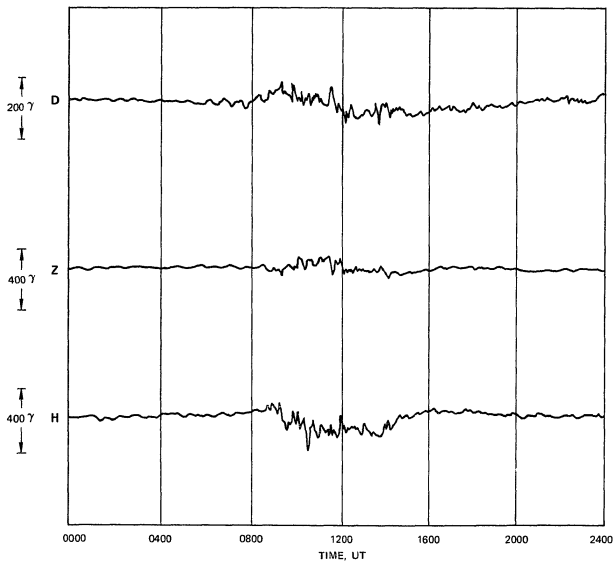
FIGURE 31   MAGNETOGRAM FOR 13 AUGUST 1975
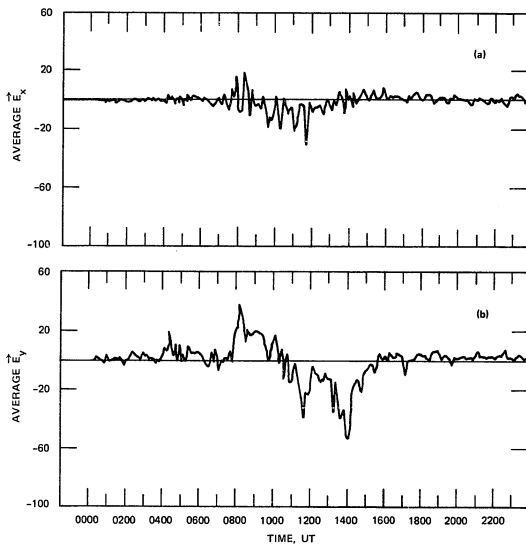
FIGURE 32 AVERAGE ELECTRIC FIELD FOR 13 AUGUST 1975. The large E_x field (~ 55 mV/m) at 1400 UT produced substantial joule heating.
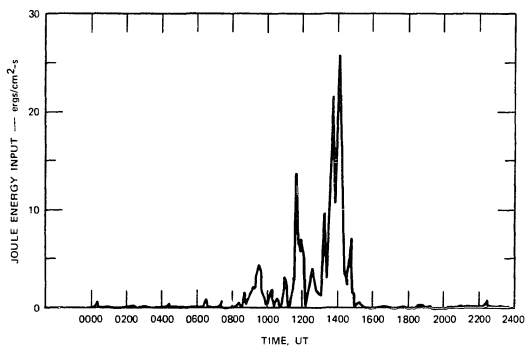
FIGURE 33   HEIGHT-INTEGRATED JOULE HEATING FOR 13 AUGUST 1975
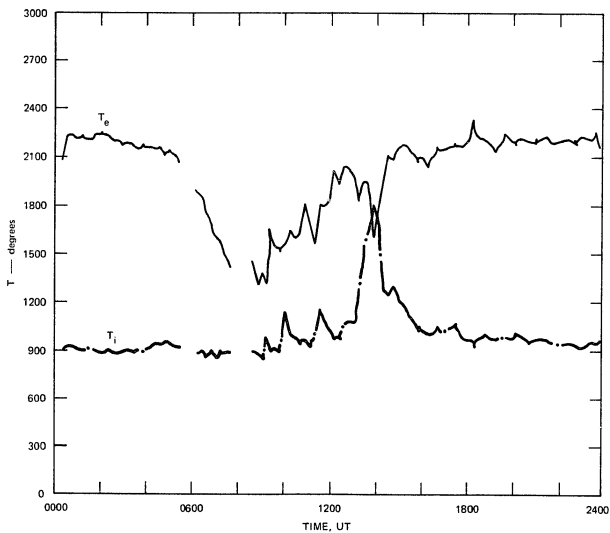
FIGURE 34   ELECTRON AND ION TEMPERATURES AT 277 km FOR 13 AUGUST 1975

with increasing SZA (from 0530 to 0800 UT). During the large joule heating event the electron temperature at this altitude appears to dip. However, these temperatures were computed assuming all O^+ ions. If heavier ions do in fact exist at 276 km during the heating period, the computed temperature will be too low. Therefore, the apparent dip in T_e is an indication that the composition was altered as high as 276 km.

The height-integrated particle energy input is indicated in Figure 35. The daytime E region is almost always present. However, particle input is apparent between 0900 and 1600 UT. The energy input between about 1200 and 1500 UT was relatively large, varying between 10 and 20 ergs/cm^2-s. The anticorrelation of particle input and large $\vec{E}$-fields is apparent at 1400 UT (when the $\vec{E}$-field is large the precipitation subsides).

The conposition contours are shown in Figure 36. The transition altitude for the first 12 hours occurs as expected (between 180 to 190 km). There is an obvious increase at 1400 UT. The transition altitude increases to 240 km and remains elevated for a number of hours. This increase of 50 km is a lower bound as described in Section III.

4. 18 February 1976

The final 24-hour period to be analyzed is by far the most active. The magnetometer data, which require "storm magnetograms," are shown in Figure 37. There are large negative bays from 0800 to 1600 UT.
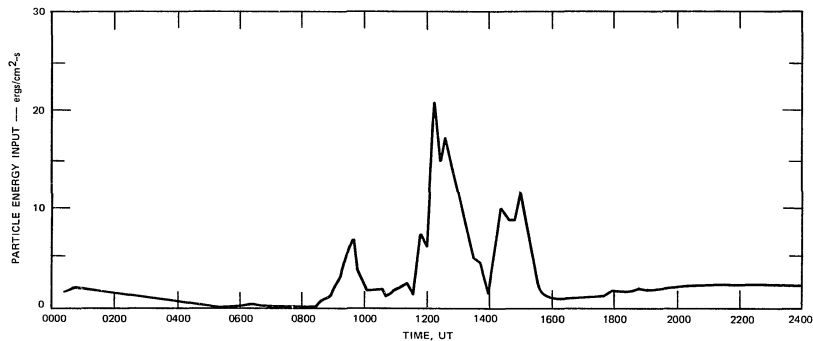
FIGURE 35   HEIGHT-INTEGRATED PARTICLE ENERGY INPUT FOR 13 AUGUST 1975
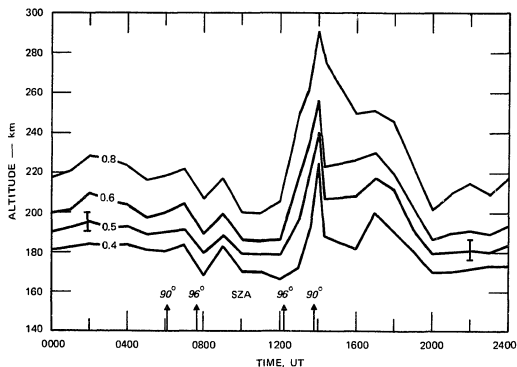
FIGURE 36   ION COMPOSITION CONTOURS FOR 13 AUGUST 1975.   At a fixed altitude the ratio of O^+ to total ionization decreased markedly during the joule heating event and increased slowly thereafter.   The transition altitude computed during the event is a lower bound with a 5 km uncertainty.
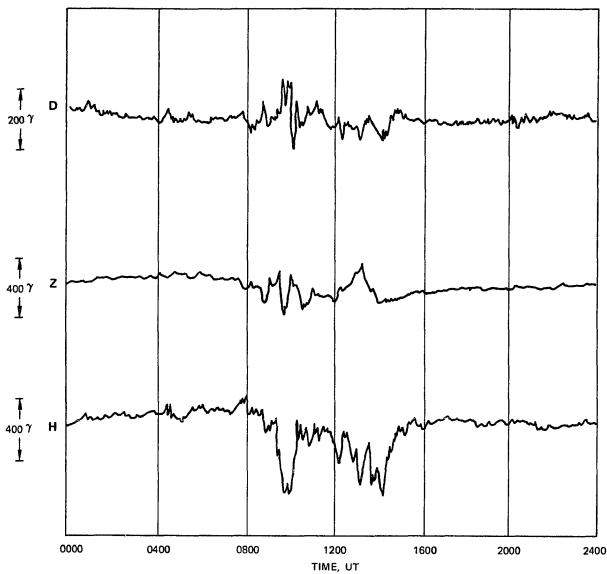
FIGURE 37   MAGNETOGRAM FOR 18 FEBRUARY 1976

The $\vec{E}$-field data are shown in the next figure (Figure 38.) The daily variation patterns are characteristic of auroral zone conditions--directed north prior to midnight, and south after midnight. The fields were occasionally large, about 50 mV/m, and the resulting joule heating was significant. A plot of the joule heating is shown in Figure 39. The joule input is often present with occasional peaks such as at 0830 and 0930 UT. The input is near zero only between 1000 UT and 1200 UT and after 1430 UT.

Energy deposition from particle precipitation is also significant. A plot of the height-integrated input is shown in Figure 40. From 0800 to 1500 UT there is nearly constant energy input of about 5 ergs/cm^2-s with occasional peaks at 20 ergs/cm^2-s corresponding to bright arcs.

The electron and ion temperatures, shown in Figure 41 are computed from the range gate corresponding to an altitude of 220 km. At the start of the run, before any auroral activity, the electron temperature is about 1500 K and decreasing (due to increasing SZA). Just after 0800 UT the electron temperature, responding to the energy input from precipitating particles, is enhanced--in fact temperatures similar to daytime conditions are reached. The temperature remains elevated until after 1500 UT, as can be seen by comparison with a quiet nighttime.

The ion temperatures also indicate the existence of energy input. At night, when the temperature is usually lower than during sunlit periods, T_i is elevated at least 100 K above the daytime temperature.
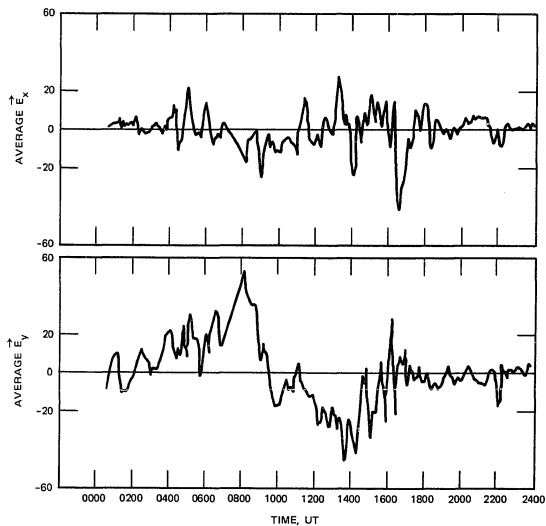
FIGURE 38 AVERAGE ELECTRIC FIELD FOR 18 FEBRUARY 1976. E_x is positive to the East; E_y is positive to the North.
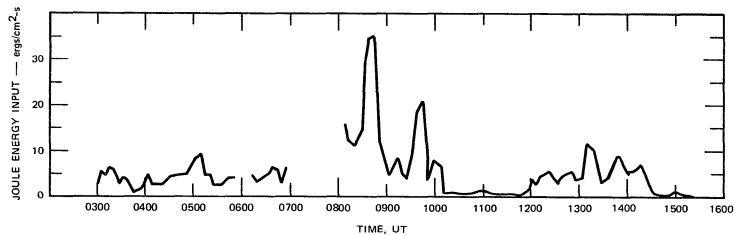
FIGURE 39   HEIGHT-INTEGRATED JOULE HEATING FOR 18 FEBRUARY 1976

74
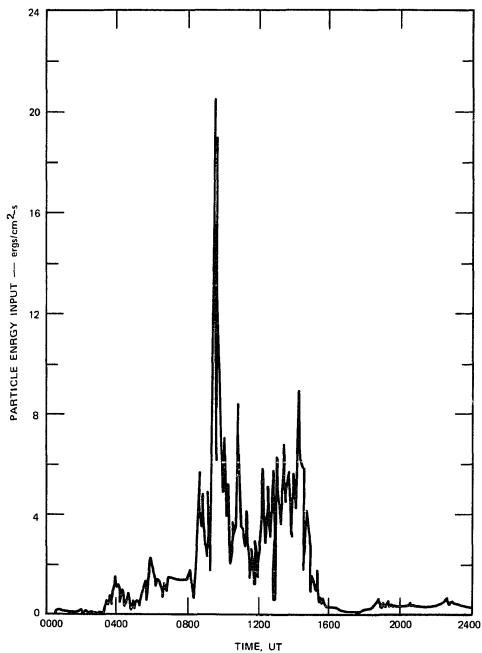
FIGURE 40   PARTICLE ENERGY INPUT FOR 18 FEBRUARY 1976
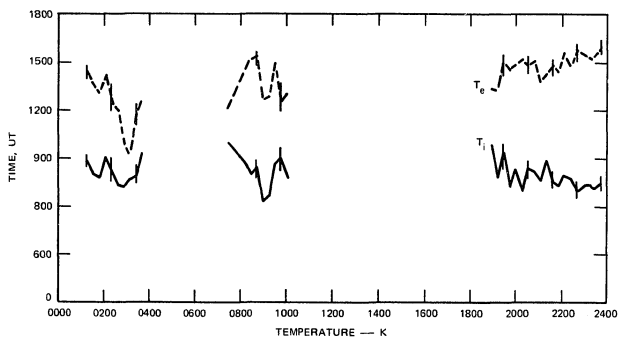
FIGURE 41   ELECTRON AND ION TEMPERATURES AT 218 km FOR 18 FEBRUARY 1976

The composition contours are shown in Figure 42. Before and after the activity transition altitude is between 180 to 190 km. During the night the joule and particle energy inputs modify the composition and the transition altitude is raised to 200 km. It is not possible to determine composition during much of the night because the F-region electron densities were too low. Consequently, the transition region data suffered from small SNR. It is apparent, however, that the composition does change such that the transition altitude is raised during the periods of enhanced ion temperatures.
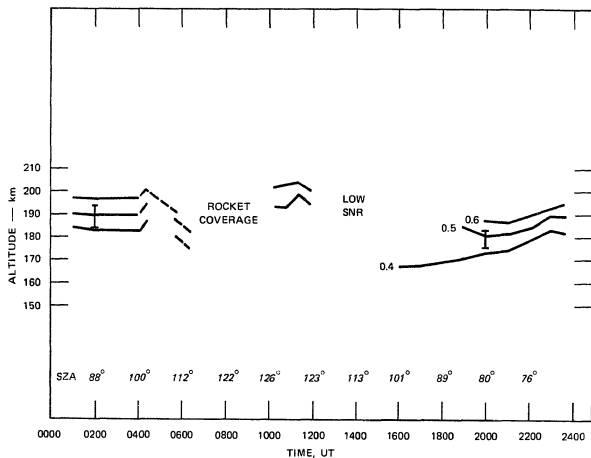
FIGURE 42   ION COMPOSITION CONTOURS FOR 18 FEBRUARY 1976

The 24-hour periods presented in the last section have been examined both for quiet-time variations of T_e, T_i, and q, and for the effects of particle precipitation and joule heating on those parameters. In order to compare the theory with the experiment, published theoretical results have been found where the conditions were similar to the experimental data.

A.   Temperature Results

1.   Quiet Periods

The daily variations of the electron and ion temperatures are determined from the quiet 24-hour periods—15 October 1975, 13 May 1976, and 18 February 1976. The October data are near the winter equinox, and consequently, the variations due to changing solar zenith angle are most pronounced. The May data represent near-solstice conditions and, as a result, little variation due to SZA is noticed.

Figure 43 shows representative daytime profiles of electron and ion temperatures in the altitude range of 160 to 275 km for the October day. F-region electron temperatures are greater than 2000 K and the ion temperatures are near 800 K.
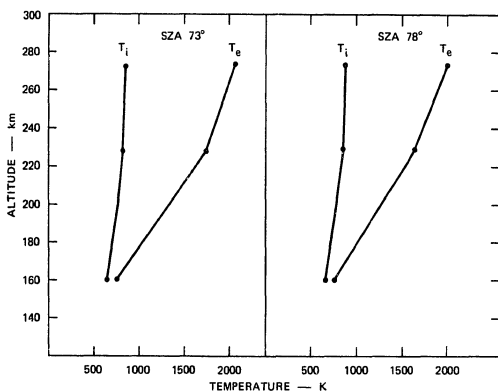
FIGURE 43   NOMINAL WINTER EQUINOX DAY (October 1975) ELECTRON AND
ION TEMPERATURE PROFILES.   At F-region heights the electron
temperature is about twice the ion temperature.

Figure 44 shows representative nighttime temperature profiles measured at times when there was little (2 to 5 ergs/cm^2-s) particle precipitation. The ion temperature profiles are similar to model T_n profiles.

The total electron temperature diurnal variation at 275 km is about 1000 K. This is consistent with diurnal variations measured at midlatitudes during sunspot minimum [Evans, 1967]. The ion temperature variation is much less--about 100 K--which is also consistent with midlatitude measurements. The CIRA 1972 model predicts exospheric temperature diurnal variations on the order of 100 K.

The second example of quiet conditions is the 13 May 1976 data. The diurnal variations due to changing solar zenith angle are much smaller because the SZA never exceeds 96° near solstice; therefore the ionosphere is continuously illuminated. Electron and ion temperature profiles for various SZAs are shown in Figure 45. There is no noticeable variation in the ion and electron temperature profiles for solar zenith angles of 55° or 75°.

A comparison of these observations with theoretical temperature profiles computed by Dalgarno and Walker [1967] shows general agreement. The T_i profiles are in good agreement; however, the T_e profiles agree in slope only. The theoretical model has generally higher temperatures. It is a difficult comparison because it is impossible to find measured electron density profiles that agree exactly with the model profiles used by Dalgarno. Agreement in T_e is best when the model electron density is lower than the measured one by about a factor of 2. The model T_e profiles are indicated in Figure 45.
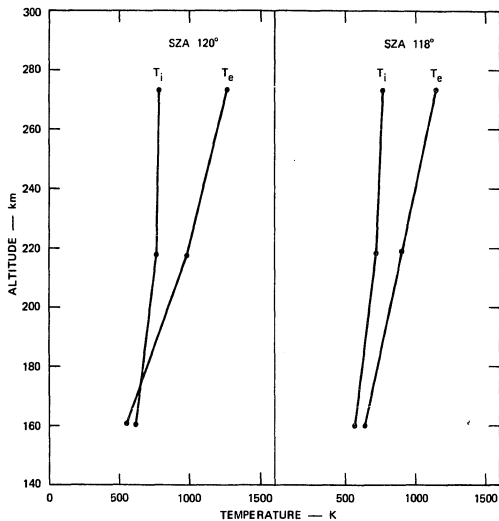
FIGURE 44   NOMINAL WINTER EQUINOX NIGHT (October 1975) ELECTRON AND ION TEMPERATURE PROFILES. The electron temperature exceeds the ion temperature indicating that some precipitation occurs even during "quiet" periods.
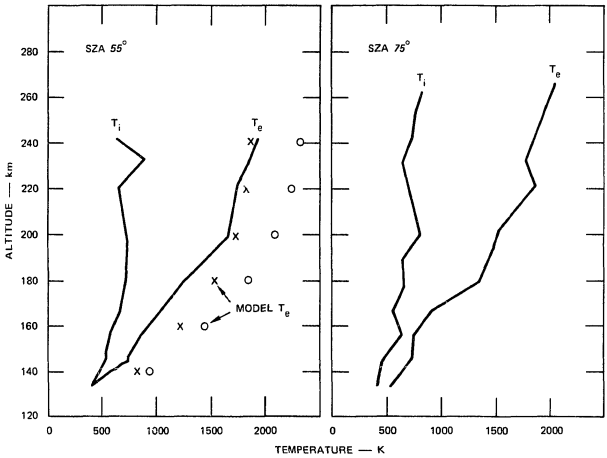
FIGURE 45 NOMINAL SUMMER SOLSTICE (May 1976) ELECTRON AND ION TEMPERATURE PROFILES. Also indicated are model temperature profiles from Dalgarno and Walker [1967].

The electron and ion temperature profiles for 18 February 1976 were computed from the daytime quiet portion of the run. They are shown in Figure 46. These winter temperature profiles have the same general appearance as the others. The T_e profile shows somewhat lower temperatures in the F region than do the May data. The T_i profiles are quite similar to the May and October data.

2. Active Periods

The energy inputs by particle precipitation and joule heating cause substantial changes in the electron and ion temperatures. The variations in temperature that were discussed previously can be overshadowed by enhancements due to auroral inputs. Rees et al. [1971] and others have studied the effects of a precipitating flux of auroral electrons on electron temperature. Their approach has been to solve the electron energy balance equation allowing for local heat sources and heat sinks and heat conduction, and assuming a reverse current equal to the primary electron flux. The calculation was performed using a model aurora. Their model was that of an intense aurora, with a total energy deposition rate of 70 ergs/cm^2-s.

A comparison between these theoretical results and electron temperatures computed from radar data is given in Figure 47. The experimental temperatures are remarkably similar to the model of Rees et al., [1971] below 200 km altitude.
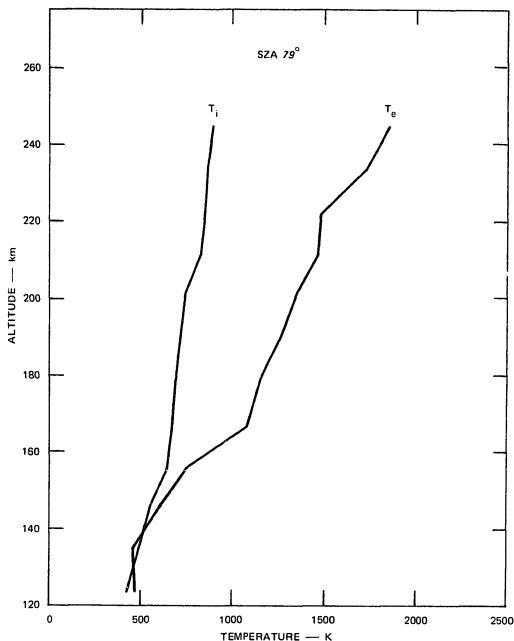
FIGURE 46   NOMINAL WINTER DAY (February 1976) ELECTRON AND ION TEMPERATURE
PROFILES.   The electron and ion temperatures are nearly equal below 140 km.
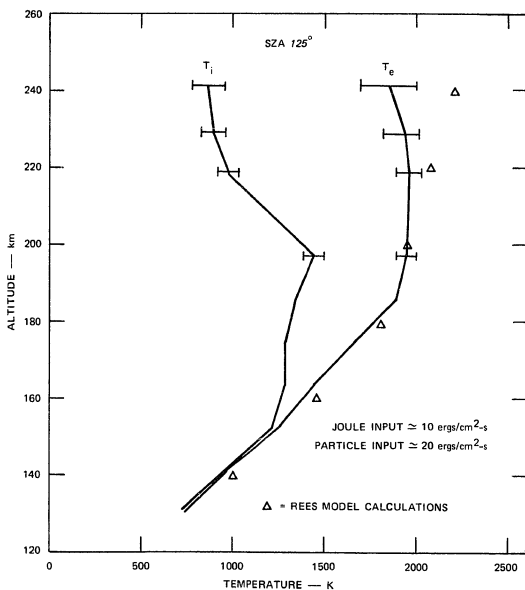
FIGURE 47   TEMPERATURE PROFILE DURING PRECIPITATION AND JOULE HEATING.
Also includes the theoretical predictions of $T_e(h)$.

On the other hand, the Rees model assumes topside heating flux and consequently predicts that $dT_e/dh > 0$ at all altitudes. As can be seen in the figure, the measured profile falls off more rapidly than in the model. Above 210 km the model T_e profile does not agree with the measurements because $dT_e/dh < 0$. Three factors could account for this:

- The heating rate would be expected to be different if the density profiles were different. The electron cooling rate is also affected because it is proportional to N_e.

- The data are taken from one antenna position-- azimuth 29° and elevation 65°; consequently the radar beam intersects magnetic field lines and the precipitation could vary with latitude.

- The Rees model does include the effects of heat flux and the conduction effects of field-aligned current. These effects are not apparent, however, at altitudes below about 250 km--i.e., the model profile with and without the heat flux and conduction appear identical below 250 km.

Another example of heating by particle precipitation is shown in Figure 48. This temperature profile is taken from the 28 February 1976 University of Texas rocket comparison. The precipitation was much less intense than in the previous example. The height-integrated energy deposition was on the order of 5 ergs/cm^2-s. The electron temperatures
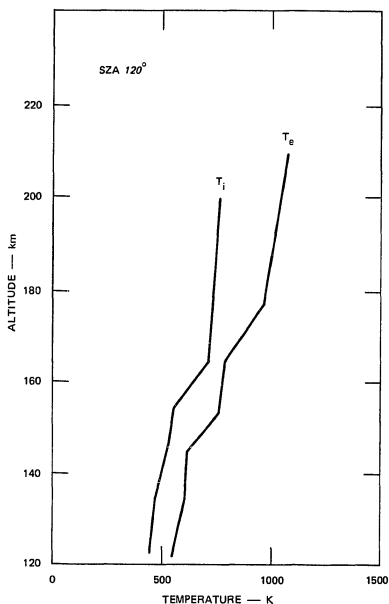
FIGURE 48   TEMPERATURE PROFILES DURING DIFFUSE PRECIPITATION
ON 28 FEBRUARY 1976.   Electron temperatures exceed the ion
temperature at all altitudes.   Height-integrated energy input was
5 ergs/cm^2-s.

are only somewhat enhanced; however, they are greater than the ion temperature at all altitudes. At 200 km the temperature is about 1000 K as compared to 2000 K for the more active night.

B. Relation Between T_i and Joule Heating

The energy input from auroral electric fields through joule heating is often the same order of magnitude as that from secondary electrons. Substantial enhancement of ion temperatures was seen in the 18 February 1976 and the 13 August 1975 data. The most dramatic event occurred on 13 August when the electric field reached 55 mV/m. The joule heating associated with that field was between 25 and 30 ergs/cm^2-s. The ion temperature for that period was enhanced by nearly a factor of 2.

Electron and ion temperature profiles computed at the peak of the energy input are shown in Figure 49. The ion temperature is greater than the electron temperature as high as 300 km. The temperatures are probably underestimated since the technique for computing the ion composition change during periods of joule heating input places a lower bound on the effect. If the electrons were heated during this period, the composition change was underestimated. Therefore, the ion temperature was probably even more enhanced than indicated.
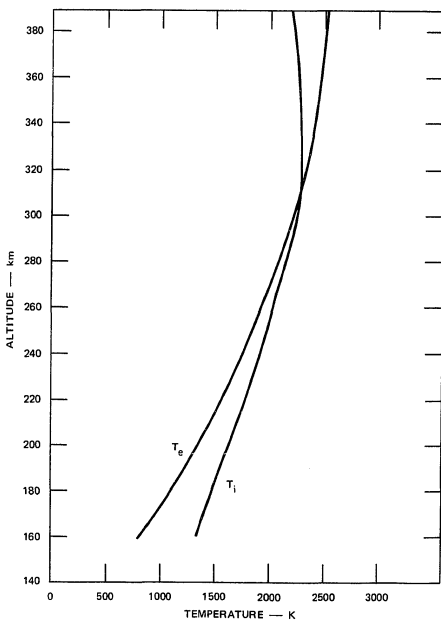
FIGURE 49   TEMPERATURE PROFILE DURING LARGE JOULE HEATING EVENT.   The ion
temperature exceeds the electron temperature below 300 km.   The joule energy
input was approximately 30 ergs/cm²-s.

C. Exospheric Temperature Variations

The exospheric temperature (T_∞) is inferred from the measured ion temperature at F-region altitudes. This is done only when no appreciable joule heating is occurring. There are two major sources of T_∞ variation. There is a diurnal variation due to solar EUV heating and there is variation due to the energy input from joule and particle heating which occurred at some time prior to the measurement.

The diurnal variation from solar EUV heating is a gradual change over the 24-hour period. This has been discussed earlier in Section V-A. Briefly the variation near equinox is about 100 K. In the summer months when the SZA is less than 96° the variation is hardly noticeable--i.e., less than the error bars (20 to 100 K for the 160-μs pulse). The deduced T_∞ generally lies between 900 and 1000 K.

The variation due to auroral inputs can be significant. The joule heating event on 13 August 1975 is a good example. The inferred exospheric temperatures show an increase of 150 K following the heating event. The temperature remains elevated for 4 to 5 hours gradually decreasing to the expected level. Figure 50 shows this temperature increase. Also shown is the ion temperature and the joule heating.

A similar increase in temperature was observed in the 13 May data, however, when there was no local auroral activity occurring. Since there was very little activity, the SNR was insufficient to compute temperatures between 0700 UT and 1500 UT. The temperature at 1500, however, was about 150 K higher than at 0700 UT. This increase cannot be attributed to EUV heating because the SZA at 0700 is nearly the same as at 1500 UT, and is
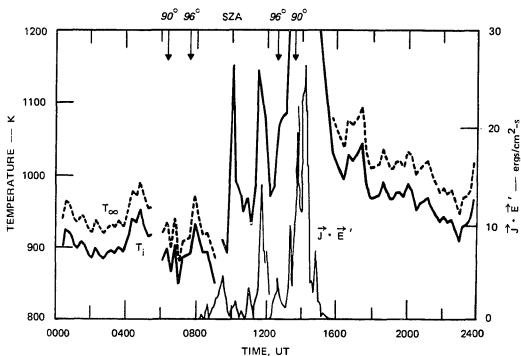
FIGURE 50 F-REGION ION TEMPERATURE, T_i, HEIGHT-INTEGRATED JOULE INPUT,
$\vec{J} \cdot \vec{E}$, AND EXOSPHERIC TEMPERATURE, T_∞, AT CHATANIKA ON 13
AUGUST 1975. The first two variables are shown in greater detail than in
the previous figure. The exospheric temperature is derived during those
periods with little or no joule heating. There is a 150-K increase in the
exospheric temperature during the night, followed by a slow decay during
the day. The ion temperatures were taken for 277 km.

> 105°. The EUV-produced maximum and minimum temperatures should occur at 0000 and 1200 UT, respectively (1400 and 0200 local time), as predicted by models--i.e., CIRA 1972.

Since there was no local heating occurring, the temperature increase must have been due to transport. Auroral activity to the north of Chatanika could be responsible for elevated neutral temperatures. The meridional neutral wind in the post-midnight sector should be directed equatorward [Nagy et al., 1974; Wickwar and Meriwether, 1978]. The warm neutral atmosphere can therefore be transported from active regions to lower latitudes.

D. Composition Results

1. Quiet Periods

The diurnal variation in the transition altitude is also determined from the undisturbed days--15 October and 13 May. The October day shows the most pronounced variation because the SZA changes significantly, while the May variations are quite small.

The October data indicate that the transition altitude increases at night. At night the altitude is greater than 190 km--generally between 190 and 200 km. During the day the transition altitude drops, and near SZA minimum it is about 175 km.

In May the SZA is never greater than 96° and not less than 45°. The transition altitude is between 190 and 200 km even when the SZA is at a minimum. The variation is consequently small--about 10 km which is on the order of the uncertainty.

These variations are in general agreement with other experimental results. The comparison will be made with the rocket data compiled by Oliver [1975]. His data represent rocket flights during quiet periods and from many locations--generally midlatitude. The May and October data indicate a decrease in transition height of 20 km from summer to winter. Oliver's rocket data also indicate such a variation. However, with so few data, only this general comparison can be made.

The diurnal variations are also in agreement with Oliver's results. Again, only a general comparison can be made because only the October data are appropriate. The radar data indicate a variation of about 15 km, the altitude being higher at night. The rocket data show a variation, however, of 30 to 40 km, again with the altitude higher at night.

This set of data in insufficient to infer a seasonal variation with any reliability; however, we can compare our results with other works. Oliver [1975] measured a summer-winter variation of about 20 km in the transition altitude, with the lowest values in the winter. He has attributed this to the effect of a higher $[O]/[N_2]$ ratio in winter (the solar zenith angle effects have been removed).

A comparison of the transition altitudes observed in May 1976 and October 1975 agree with the seasonal trend observed by Oliver. The transition altitudes were compared at times where the SZA was the same. For example, for the SZA equal to 72° the May data indicate that the transition altitude was about 193 km, whereas in October it was 175 km.

This would support the idea of a change in the $[O]/[N_2]$ ratio even at higher latitudes [Roble, 1977].

2. **Active Periods**

Variations in ion composition have also been observed that are not associated with seasonal effects or solar EUV heating. During periods of large energy input the composition can be significantly modified. The active periods of both 13 August and 18 February show the effects of auroral energy inputs on composition.

The 13 August data shown in Section IV indicate a substantial increase in the transition altitude during a joule heating event. The energy input at the time was large--30 $ergs/cm^2$-s. The transition altitude increased from 180 km to 240 km. Just prior to the large joule input, there were moderate levels of particle inputs--about 20 $ergs/cm^2$-s. However, as the $\vec{E}$-field became large, the precipitation subsided. The composition change was not obvious until after 1300 UT which is during the precipitation decrease and the joule heat increase. The transition altitude was not affected by precipitation alone.

The F-region ion temperature exceeded 2200 K at 335 km and was greater than the electron temperature at altitudes below 300 km. As a result, various factors contribute to modify the composition. The reaction rate ($O^+ + N_2$) is enhanced, consequently, the electron density is reduced. The decay of ionization in the F region during the event is shown in Figure 51. The result is a dramatic increase in transition
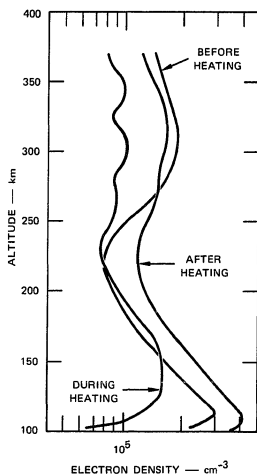
FIGURE 51   ELECTRON DENSITY PROFILES DURING THE JOULE HEATING EVENT ON 13 AUGUST 1975. The F-region density decreases during the event and then recovers as the heating subsides.

altitude, i.e., the function q is strongly dependent on electron density. Enhanced $[N_2]$ resulting from the heating is also a contributing factor to the composition change, however, the effect would be small since the neutral temperature enhancement was only 150 K. ($[N_2]$ at 300 km would increase by less than a factor of 2.)

E. Numerical Modeling of Transition Altitude Variation

The effects of all of the factors described in this section are evaluated by modeling the composition profiles under various conditions. The conditions include quiet day and night parameters in order to establish background composition profiles. The effects of precipitation, joule heating, and seasonal variation of $[N_2]$ can be examined. These factors can be examined with the aid of an expression derived using the following simplified system of reactions and continuity equations:

$$O^+ + O_2 \xrightarrow{\gamma_1} O_2^+ + O$$

$$O_2^+ + e \xrightarrow{\alpha_1} O + O$$

$$O^+ + N_2 \xrightarrow{\gamma_2} NO^+ + N$$

$$NO^+ + e \xrightarrow{\alpha_2} N + O$$

$$N_2^+ + O \xrightarrow{\gamma_3} NO^+ + N$$

$$N_2^+ + e \xrightarrow{\alpha_3} N + N$$
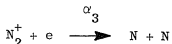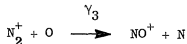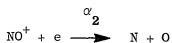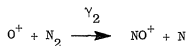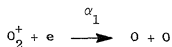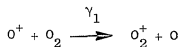
$$\frac{\partial [O^+]}{\partial t} = q(O^+) - \gamma_1 [O_2][O^+] - \gamma_2 [N_2][O^+] = 0$$

$$\frac{\partial [NO^+]}{\partial t} = \gamma_2 [N_2][O^+] + \gamma_3 [N_2^+][O] - \alpha_2 [NO^+]N_e = 0$$

$$\frac{\partial [O_2^+]}{\partial t} = q(O_2^+) + \gamma_1 [O_2][O^+] - \alpha_1 [O_2^+]N_e = 0$$

$$\frac{\partial [N_2^+]}{\partial t} = q(N_2^+) - \gamma_3 [N_2^+][O] - \alpha_3 [N_2^+]N_e = 0$$

where $q(x)$ is the production rate of species x. If steady state is assumed, the number densities of the various ions are expressed as:

$$[NO^+] = \frac{\gamma_2 [N_2][O^+]}{\alpha_2 N_e} + \frac{\gamma_3 [N_2^+][O]}{\alpha_3 N_e}$$

$$[O_2^+] = \frac{q(O_2^+) + \gamma_1 [O_2][O^+]}{\alpha_3 N_e}$$

$$[N_2^+] = \frac{q(N_2^+)}{\gamma_3 [O] + \alpha_3 N_e} \qquad .$$

Substitution of the above into the expression for charge neutrality,

$$N_e = [O^+] + [NO^+] + [O^+]$$

and solving for $[O^+]/N_e$, gives

$$\frac{[O^+]}{N_e} = \cfrac{1}{\cfrac{\gamma_1[O_2] + \gamma_2[N_e]}{q(O^+)}\left[\cfrac{\gamma_3[N_2^+][O]}{\alpha_2 N_e} + \cfrac{q(O_2^+)}{\alpha_1 N_e}\right] + \cfrac{\gamma_2[N_2]}{\alpha_2 N_e} + \cfrac{\gamma_1[O_2]}{\alpha_1 N_e} + 1}$$

where

$$q(O^+) = \frac{0.56[O]\eta}{1.15[N_2] + 1.5[O_2] + 0.56[O]}$$

$$q(O_2^+) = \frac{[O_2]\eta}{1.15[N_2] + 1.5[O_2] + 0.56[O]}$$

$$[N_2^+] = \frac{q(N_2^+)}{\gamma_3[O] + \alpha_3 N_e}$$

$$= \left[\frac{0.92[N_2]\eta}{1.15[N_2] + 1.5[O_2] + 0.56[O]}\right] / (\gamma_3[O] + \alpha_3 N_e)$$

and η = total ion production rate [Jones and Rees, 1973]. The effects on the transition altitude of varying the atmospheric density, electron density, production rate, and temperature can then be assessed.

1. **Quiet Conditions--Diurnal Variation**

The model atmosphere used in all cases was taken from Banks and Kockarts for an exospheric temperature of 1000 K, and the ionospheric parameters were obtained from Chatanika radar data. The model atmospheric and ionospheric data are given in Table 4. The composition profiles are shown in Figure 52. The difference in the profiles is most pronounced above 180 km. Above that altitude, the daytime electron density is at least an order of magnitude larger than the nighttime density. The transition altitude increases by about 20 km at night.

2. **Active Conditions--Particle Precipitation**

The effects of electron precipitation that are considered are enhanced N_e, electron temperature, and vibrational temperature of N_2. The atmospheric and ionospheric parameters are given in Table 5. The first case considered uses temperature and N_e profiles from data taken on 18 February 1976. The particle energy input was approximately 20 ergs/cm^2-s. The composition profiles shown in Figure 53 indicate that, relative to the background profile (quiet night), the transition altitude is lower by more than 20 km. In fact, the transition altitude is lower in this case than it was using daytime conditions.

The effects of enhanced vibrational temperatures of N_2 are examined using the above (active night) model. According to Schunk and Banks [1975], the vibrational temperatures during an auroral substorm can be in the range 1400 to 2200 K. These temperatures will increase the

Table 4

MODEL ATMOSPHERE AND IONOSPHERIC DATA FOR QUIET DAY AND NIGHT

Quiet Day

Alt (km)	N_e (cm^{-3})	T_i (K)	T_e (K)	$[O_2]$ (cm^{-3})	$[O]$ (cm^{-3})	$[N_2]$ (cm^{-3})
140	7.5E4*	596	650	4.40E9	2.44E10	5.37E10
160	1.0E5	765	1000	1.20E9	1.13E10	1.67E10
180	1.2E5	861	1600	4.43E8	6.45E9	6.88E9
200	1.5E5	916	1800	1.87E8	4.07E9	3.22E9
220	2.0E5	948	2000	8.48E7	2.69E9	1.60E9
240	3.0E5	967	2000	4.00E7	1.83E9	8.26E8
260	2.5E5	979	2000	1.93E7	1.26E9	4.36E8
280	2.45E5	986	2000	9.43E6	8.80E8	2.33E8
300	2.0E5	991	2000	4.67E6	6.20E8	1.26E8

Quiet Night

Alt (km)	N_e (cm^{-3})	T_i (K)	T_e (K)	$[O_2]$ (cm^{-3})	$[O]$ (cm^{-3})	$[N_2]$ (cm^{-3})
140	8.6E4	596	596	4.40E9	2.44E10	5.37E10
160	7.0E4	765	765	1.20E9	1.13E10	1.67E10
180	5.6E4	861	861	4.43E8	6.45E9	6.88E9
200	5.0E4	916	916	1.87E8	4.07E9	3.22E9
220	3.4E4	948	948	8.48E7	2.69E9	1.60E9
240	3.0E4	965	965	4.00E7	1.83E9	8.26E8
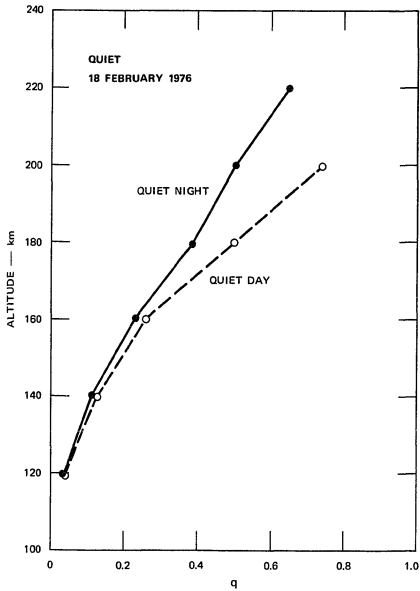
FIGURE 52   MODEL COMPOSITION PROFILES SHOWING DIURNAL
VARIATION

Table 5

MODEL ATMOSPHERE AND IONOSPHERIC DATA FOR ACTIVE (AURORA) NIGHT

Alt (km)	N_e (cm^{-3})	T_i (K)	T_e (K)	$[O_2]$ (cm^{-3})	$[O]$ (cm^{-3})	$[N_2]$ (cm^{-3})
140	2.0E5	596	750	4.40E9	2.44E10	5.37E10
160	1.3E5	765	1120	1.20E9	1.13E10	1.67E10
180	1.5E5	861	1300	4.43E8	6.45E9	6.88E9
200	1.8E5	916	1800	1.87E8	4.07E9	3.22E9
220	1.9E5	948	2000	8.48E7	1.83E9	1.60E9
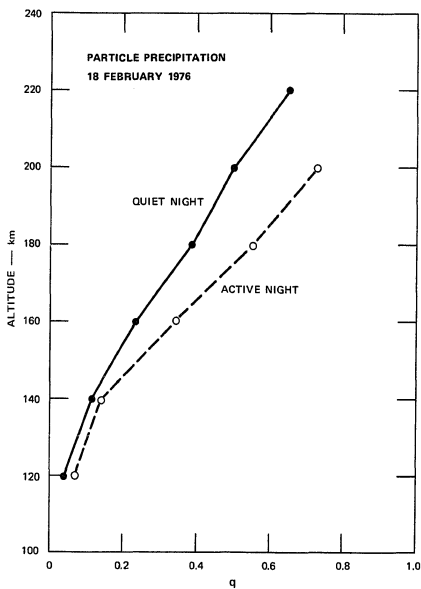
FIGURE 53   MODEL COMPOSITION PROFILES SHOWING THE EFFECTS
OF AURORAL IONIZATION

N_2 and O^+ reaction-rate coefficient by 1.5 to 3.6 times the ground-state coefficient. Consequently, the composition profiles were recomputed applying those factors to γ_2. The results are shown in Figure 54. There is a substantial increase in the transition altitude for the case when $T_v = 2200$ K.

3. Effect of Joule Heat Input

The atmospheric model and ionospheric data used to evaluate the effect of joule heat are given in Table 6. The ionospheric data, electron density, and electron and ion temperatures were taken from 13 August 1975 data. The composition profile (Figure 55) corresponding to the active data indicates that more molecular ions exist at all altitudes as compared to the quiet period. The transition altitude increased by 20 km. The active period was characterized by elevated ion temperature and decreased electron density; both factors contribute to the increase of the transition altitude.

4. Effect of Seasonal Variation of $[N_2]$

The horizontal neutral winds resulting from global circulation cause a variation in the number density of N_2 as a function of season [Roble, 1977]. This variation is such that at solstice $[N_2]$ is enhanced in the summer hemisphere and depleted in the winter hemisphere. The effect of this variation on ion chemistry can be seen in the quiet-time transition altitude.
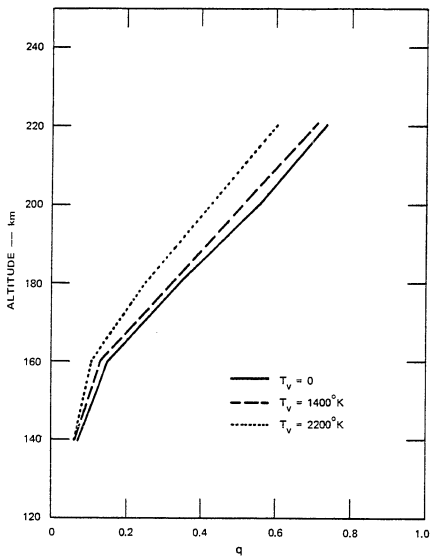
FIGURE 54   COMPOSITION PROFILES SHOWING THE EFFECT OF ENHANCED N_2 VIBRATIONAL TEMPERATURE. The model from Table 9 was used and the reaction-rate coefficient for $N_2 + O^+$ was enhanced.

Table 6

MODEL ATMOSPHERE AND IONOSPHERIC DATA USED TO EVALUATE

THE EFFECT OF JOULE HEAT

Active Day (Joule Heating)

Alt (km)	N_e (cm^{-3})	T_i (K)	T_e (K)	$[O_2]$ (cm^{-3})	$[O]$ (cm^{-3})	$[N_2]$ (cm^{-3})
160	2.0E5	830	965	1.20E9	1.13E10	1.67E10
190	1.2E5	1050	1400	2.85E8	5.08E9	4.66E9
220	1.5E5	1200	2000	8.48E7	2.69E9	1.60E9
276	1.0E5	1800	2000	9.60E6	9.00E8	2.50E8

Quiet Day

Alt (km)	N_e (cm^{-3})	T_i (K)	T_e (K)	$[O_2]$ (cm^{-3})	$[O]$ (cm^{-3})	$[N_2]$ (cm^{-3})
160	2.0E5	765	965	1.20E9	1.13E10	1.67E10
190	2.3E5	1100	1784	2.85E8	5.08E9	4.66E9
220	3.5E5	1600	2000	8.48E7	2.69E9	1.60E9
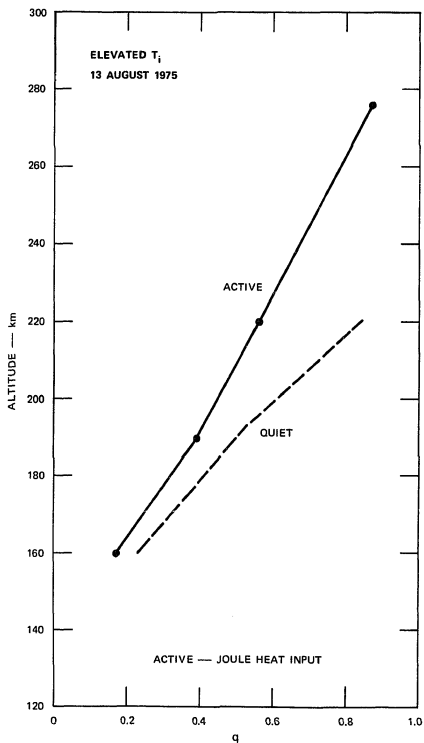
FIGURE 55   COMPOSITION PROFILE CORRESPONDING TO THE JOULE HEAT INPUT COMPARED TO THE QUIET PERIOD

The model used to compute the transition altitude is shown in Table 7. In this model the parameters are identical to the quiet-day model used earlier, corresponding to the February 18 data. However, in this case the $[N_2]$ was increased above 160 km by an incremental amount to a factor-of-2 enhancement at 300 km. The effect can readily be seen in Figure 56. The relative abundance of molecular ions increased with enhanced $[N_2]$. The transition altitude increased by approximately 5 km.

Table 7

MODEL ATMOSPHERE AND IONOSPHERIC DATA USED

TO EVALUATE THE EFFECT OF ENHANCED $[N_2]$

Alt (km)	N_e (cm^{-3})	T_i (K)	T_e (K)	$[O_2]$ (cm^{-3})	$[O]$ (cm^{-3})	$[N_2]$ (cm^{-3})
140	7.5E4	596	650	4.40E9	2.44E10	5.37E10
160	1.0E5	765	1000	1.20E9	1.13E10	1.67E10
180	1.2E5	861	1600	4.43E8	6.45E9	7.90E9
200	1.5E5	916	1800	1.87E8	4.10E9	4.19E9
220	2.0E5	948	2000	8.48E7	2.70E9	2.32E9
240	3.0E5	967	2000	4.00E7	1.80E9	1.32E9
260	2.5E5	979	2000	1.93E7	1.26E9	7.63E8
280	2.4E5	986	2000	9.43E6	8.80E8	4.43E8
300	2.0E5	991	2000	4.67E6	6.20E8	2.52E8
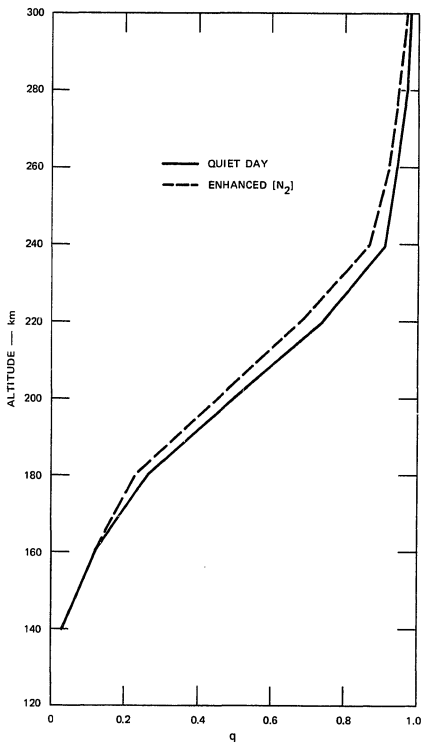
FIGURE 56   COMPOSITION PROFILES SHOWING THE EFFECT OF ENHANCED $[N_2]$ ABOVE 160 km

F.   Time Dependence of Joule Heating and Ionic Composition Changes

During periods of large perpendicular electric fields, the temperature difference $(T_i - T_n)$ resulting from frictional heating is quickly established. The time required is inversely proportional to the ion-neutral collision frequency. In the F-region this time is on the order of one second or less. Although both the ions and neutrals are heated, a temperature difference exists as long as the heating source is present. When the heat source subsides, the ions quickly lose their excess thermal energy to the neutrals, reestablishing thermal equilibrium below about 300 km. The resulting neutral-gas temperature is therefore enhanced.

Enhanced ion and neutral temperatures were observed during the August 1975 joule heating event. The temperature remained elevated for nearly eight hours. Although the resulting modification of the ion composition was greatest during the heating period, it persisted for about 6 to 8 hours. The decay of F-region temperatures was gradual over that period--decreasing from about 1050 K to about 900 K. This decay time is quite long--with no heat source, elevated ion temperature should decrease much more quickly. Evans [1965] measured ion temperatures during a solar eclipse and found T_i to decrease 200 K within 1 to 2 hours. Consdquently, the August 1975 data suggest that non-local heating was occurring just after the joule heating event. As mentioned earlier, southward meridional winds could cause the observed effect--i.e., the elevated temperatures are produced by activity to the north of Chatanika and the heated atmosphere is transported by the neutral wind. These winds are typically directed south during the night and turn northward in the morning near 1000 AST [Wickwar and Meriwether, 1978].

VI   SUMMARY AND CONCLUSIONS

The results of the first continuous long-term (24-hour) measurements of ionospheric temperatures and composition at high latitudes have been presented. The use of the incoherent-scatter radar technique has been demonstrated as particularly well suited for these experiments. The effects of auroral processes were observed throughout the evolution of the entire substorm. In addition, quiet-time observations of the same parameters were made and compared to midlatitude observations.

Dramatic increases in temperatures were observed during periods of particle precipitation and large electric fields. Increases in electron temperatures on the order of 1000 K were observed at night when the energy deposition rate was 20 ergs/cm^2-s. These increases are consistent with theory. Similar increases in ion temperature were observed during joule heating events. At F-region altitudes the ion temperature more than doubled during a period when the energy input was 30 ergs/cm^2-s.

Electron and ion temperature profiles were measured during periods of no auroral energy input. From these measurements, the diurnal variations were determined. It was found that the profiles and the variations are similar to those measured at midlatitudes. The response of the electron temperatures to the changing SZA is as much as 1000 K. The ion temperatures vary by 100 K for the same SZA change.

112

Exospheric temperatures were deduced and found to be between 800 and 1000 K. These low temperatures can be expected during sunspot minimum, and agree with midlatitude data [Alcayde et al., 1974]. Variations in T_∞ over 24 hours do not exceed 100 K. However, the effects of heat inputs and possibly transport of heated neutrals have been observed. The T_∞ increased by 150 K following a large joule heating event of 30 ergs/cm^2-s. Similar increases have been seen when no $\vec{E}$-fields were present, suggesting that transport by meridional neutral winds could be responsible for the observation.

One of the main points of this experiment was the determination of the relative abundance of O^+ ions, as compared with molecular ions (NO^+ and O_2^+). It was found that, during the quiet periods, the ionic composition in the high-latitude ionosphere is similar to midlatitude composition. The transition altitude (the altitude where half of the ions are O^+) occurs near 190 km during the night in the winter and near 170 km during the day--a diurnal variation due to variation of the solar EUV ionization. In summer the transition altitude occurs near 190 km during most of the day and night. The SZA does not exceed about 96°; consequently, no detectable diurnal variation occurs. The difference in the altitudes from summer to winter (for the same SZA) is also similar to that observed at midlatitudes. This indicates that the $[O]/[N_2]$ seasonal variation exists also at high latitudes, resulting from global circulation patterns.

There are substantial departures from these observations during joule heating events. The transition altitude was observed to increase by 50 km during the 13 August 1975 event. Similar increases were seen in the 18 February 1976 data. These effects have been theoretically predicted by Schunk et al. [1976], and others. A change in the reaction-rate coefficients and a change in the neutral composition due to the elevated temperatures are likely to cause the change in ionic composition.

This work has been an exploratory study of the effects of auroral energy inputs into the ionosphere and the development of a technique to investigate them. We are presently developing techniques that will allow a more sophisticated sequence of pulses to be analyzed. This will allow us to use short pulses suited for E and F_1 regions and long pulses suited for F region altitudes simultaneously, thus providing optimum resolution and signal strength. We expect that this hybrid technique will eliminate the loss of data continuity that occurs with low-SNR situations when using short pulses, and the loss of data that is unavoidable below 160 km when using long pulses.

APPENDIX

ERROR ANALYSIS

115

APPENDIX

ERROR ANALYSIS

1. Temperature--Statistical Error

Statistical uncertainties in T_i and T_r exist as a result of performing a least-squares fit of a theoretical ACF with experimentally measured ACFs. The goodness of fit depends on the quality of the measured ACF--i.e., good or poor SNR.

The formulation used in this dissertation was originally developed by Waldteufel at Arecibo and was adapted for use at Chatanika by Wickwar [1974]. The fitting procedure attempts to minimize the function:

$$\chi^2(x_j) = \sum_n (1/\sigma_n^2 \ [TACF_n(s_j) - XACF_n]^2)$$

where

$\quad\quad x_j$ = Parameters to be determined

$\quad\quad TACF_n$ = Theoretical autocorrelation function

$\quad\quad XACF_n$ = Experimental autocorrelation function

$\quad\quad \sigma_n^2$ = Variance of each lag[*]

$\quad\quad n$ = 1, 2, ... , N = lag number.

---

[*] Footnote is on the following page.

116

*

$$\sigma_n^2 = \frac{1}{K} \left\{ \left[1 + \frac{N}{S} \right]^2 + \left[XACF_S + \frac{N}{S} XACF_N \right]^2 \right\} + \frac{1}{K_N} \left\{ \frac{N}{S} \right\}^2 \left\{ 1 + XACF_N^2 \right\}^2$$

where

K = Number of frames/signal samples (integrated)

K_N = Number of noise samples

N, S = Noise and Signal power

$XACF_S$ = Signal ACF's

$XACF_N$ = Noise ACF's.

This expression is taken from Farley [1969].

The fitting procedure begins by expanding the $TACF_n(x_j)$ in a Taylor series:

$$TACF_n(x_j + \delta x_j) \approx TACF_n(x_j) + \sum_j \frac{\partial TACF_n(x_j)}{\partial x_j} \delta x_j$$

and substituting the result in the χ^2 expression. Now, if $\chi^2(x_j)$ is to be a minimum, then

$$\frac{\partial [\chi^2(x_j)]}{\partial x_j} = 0 \quad .$$

For example, in terms of the parameter x_ℓ,

$$\frac{\partial [\chi^2(x_j)]}{\partial x_\ell} = 2 \left\{ \sum_n \frac{1}{\sigma_n^2} [TACF_n(x_j) - XACF_n] \frac{\partial TACF_n(x_j)}{\partial x_\ell} \right.$$

$$\left. + \sum_j \sum_n \frac{1}{\sigma_n^2} \frac{\partial TACF_n}{\partial x_j} \frac{\partial TACF_n}{\partial x_\ell} \delta x_j \right\} = 0 \quad .$$

Repeating this for all parameters leads to a system of equations that can be expressed in matrix form as:

$$\overline{Z} + \overline{\overline{S}} \cdot \overline{\delta x} = 0$$

where

$$\bar{Z} = \sum_n \frac{1}{\sigma_n^2} [TACF_n(x_j) - XACF_n] \frac{\partial TACF_n(x_j)}{\partial x_\ell}$$

$$\bar{\bar{S}} = \sum_j \sum_n \frac{1}{\sigma_n^2} \frac{\partial TACF_n}{\partial x_j} \frac{\partial TACF_n}{\partial x_\ell} \quad .$$

Given a set of initial parameters, x_i, the corrections required to approximate x_j are the δx_j's. Solving the matrix equation above for $\overline{\delta x}$ gives

$$\delta x = -\bar{\bar{S}}^{-1} \cdot \bar{Z} \quad .$$

The errors are contained in the error matrix $\bar{\bar{S}}^{-1}$. An example of the random error of ion temperature as a function of signal-to-noise ratio is shown in Figure A-1. Data were processed for this dissertation using a SNR threshold of 0.15 .

2. Temperature--Systematic Error

In addition, systematic errors exist as a result of making the measurements over pulse lengths as long as 48 km. These errors depend on the gradients of the measured parameters and on the weighting effect of the gradient of the electron density.

The possible effect of pulse-length smearing is that the average temperature over the 48-km region may not be the temperature at the midpoint of the pulse. In order to investigate this uncertainty, the following procedure was used:
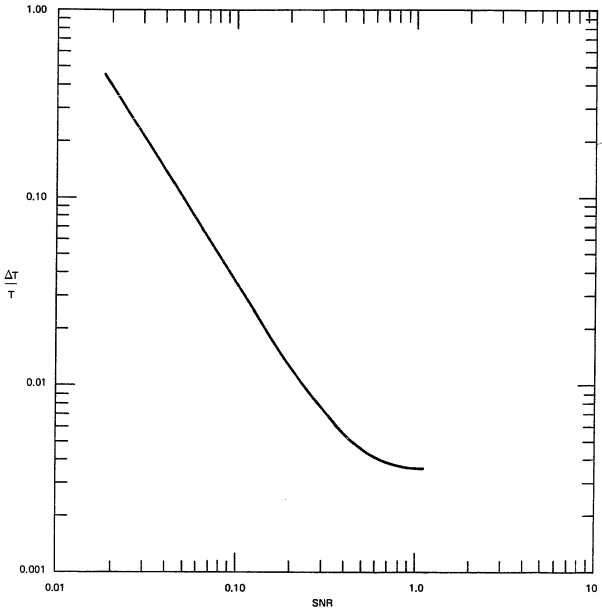
FIGURE A-1   TEMPERATURE UNCERTAINTY USING THE LONG-PULSE
CORRELATOR--10-MINUTE INTEGRATION TIME

(1) Compute temperature profiles for both day and
    night temperature gradients.

(2) Compute the weighted average temperature sampling
    at 4-km intervals over the 48-km pulse length.

(3) Determine the altitude that corresponds to the
    weighted average temperature.

(4) Compare the above altitude with the midpoint
    altitude.

In order to compute the weighted average temperature for samples spaced
at 4-km intervals over the 48-km region corresponding to a pulse length,
the following equation was used to determine the weighted temperature:

$$T = \frac{\sum\limits_{j=6}^{13} j w_j T_i + \sum\limits_{j=14}^{20} (26 - j) w_j T_i}{\sum\limits_{j=6}^{13} j w_j + \sum\limits_{j=14}^{20} (26 - j) w_j}$$

where

$$w = N_e (R_o/R)^2 \quad .$$

The weighting function, w, weights the temperature samples according to
the received power, referenced to the center of the 48-km pulse, R_o--
i.e., for values closer than the center of the pulse $(R_o/R) > 1$. The
additional weighting, $\sum\limits_{j=6}^{13} j$, $\sum\limits_{j=14}^{20} (26 - j)$, takes into account the tri-
angular weighting of the autocorrelation technique. Contributions from
values < 6 and > 20 were negligible. Examples of the errors are given
in Figure A-2.
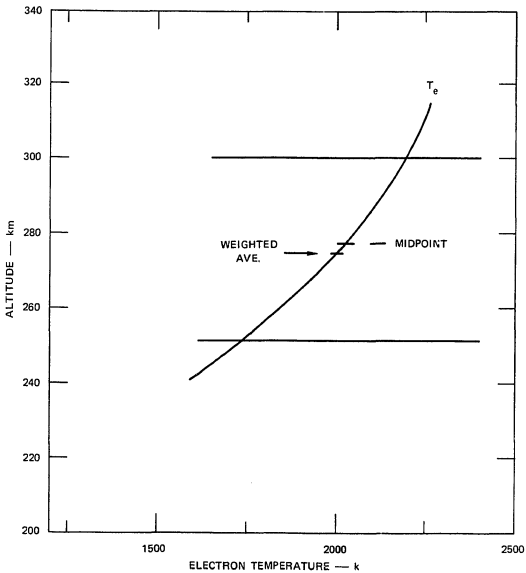
FIGURE A-2   WEIGHTED AVERAGE TEMPERATURE COMPARED TO THE MIDPOINT OF THE PULSE. The T_e gradient was taken from the 13 August 1975 joule heating event.

3. Composition--Statistical Error

Statistical uncertainties in the ion composition results arise from the statistical uncertainties in the temperature data. As described in Section III-B, the ion temperature for an unknown ion mass is related to the ion temperature for O^+ ions by the following relation:

$$T(q) = A(q)T(1)$$

where q is the fraction of O^+ ions.

$$A(q) = \frac{T(q)}{T(1)}$$

$$\frac{\partial A(q)}{\partial T(q)} = \frac{1}{T(1)}$$

$$\sigma A(q) = \frac{\sigma T(q)}{T(1)} \quad .$$

for a given q, the uncertainty in A(q) is $\Delta T/T$, where ΔT is the statistical error given in the previous section.

4. Composition--Systematic Error

There are two sources of systematic errors in composition:

(1) The ion temperature uncertainty will result in an
    uncertainty in the choice of T_∞. As a result, the
    T_n profile used in the analysis could have a system-
    atic error. This error is minimized by fitting as
    many data points as possible at altitudes where q
    can safely be assumed to be 1.

(2) The CIRA 72 neutral atmospheric model may not
    accurately represent the high-latitude atmosphere.
    At altitudes less than 140 km, the measured ion
    temperatures were always greater than the model T_n.
    This effect cannot be a result of an error in the
    composition because there are a negligible number
    of atmoic ions at altitudes less than 140 km.

REFERENCES

125

REFERENCES

Alcayde, D., P. Bauer, and J. Fontanari (1974), "Long-Term Variations of
    Thermospheric Temperature and Composition," J. Geophys. Research,
    Vol. 79, No. 4, pp. 629-637.

Banks, P. M. and G. Kockarts, Aeronomy, pp. 329-338 (Academic Press,
    New York, N.Y., 1973).

Banks, P. M., R. W. Schunk and W. J. Raitt (1974), "NO^+ and O^+ in the
    High-Latitude F-region," Geophys. Res. Letters, Vol. 1, pp. 239-242.

Baron, M. J., O. de la Beaujardiere, and B. Craig (1970), "Project 617
    Radar--Readiness Achievement Program, Part A--Data Processing and
    Analysis," Contract DASA 01-67-C-0019, Stanford Research Institute,
    Menlo Park, CA.

Bowles, K. L. (1958), "Observations of Vertical Incidence Scatter from
    the Ionosphere at 41 Mc/sec," Phys. Rev. Letters, Vol. 1, pp. 454-
    455.

Brekke, A. and C. L. Rino (1978), "High-Resolution Altitude Profiles of
    the Auroral Zone Energy Dissipation due to Ionospheric Currents,"
    J. Geophys. Research, Vol. 83, No. A6, pp. 2517-2524.

Carru, H., M. Petit, and P. Waldteufel (1967), "1967 Mesures de Tempera-
    tures Electroniques et Ioniques par Diffusion Incoherente,"
    J. Atmos. Terr. Phys., Vol. 29, No. 4, pp. 351-366.

CIRA 1972. COSPAR International Reference Atmosphere 1972, Compiled by
    COSPAR Working Group 4, Akademie-Verlag, Berlin.

CIRA 1965. CIRA COSPAR International Reference Atmosphere, Compiled by
    COSPAR Working Group IV, North Holland Publishing Co., Amsterdam.

Dalgarno, A. and J. C. G. Walker (1967), "Ion Temperatures in the Top-
    side Ionosphere," Planet. Space Science, Vol. 15, pp. 200-203.

Dougherty, J. P., and D. T. Farley (1960), "A Theory of Incoherent
    Scattering of Radio Waves by a Plasma," Proc. Roy. Soc. A, Vol. 259,
    pp. 79-99.

Evans, J. V. and W. L. Oliver (1972), "The Study of E-Region Ion Concen-
    tration and Composition by Incoherent Scatter Radar," Radio Science,
    Vol. 7, pp. 103-112.

REFERENCES (continued)

Evans, J. V. and L. P. Cox (1970), "Seasonal Variation of the F_1-Region
    Ion Composition," J. Geophys. Research, Vol. 75, pp. 159-164.

Evans, J. V. (1967), "Midlatitude F-Region Densities and Temperatures at
    Sunspot Minimum," Planet. Space Science, Vol. 15, pp. 1387-1405.

Evans, J. V. (1965), "An F Region Eclipse," J. Geophys. Research, Vol. 70,
    pp. 131-142.

Farley, D. T. (1969), "Incoherent Scatter Correlation Function Measure-
    ment," Radio Sci., Vol. 4, No. 2, P. 143.

Fejer, J. A. (1961), "Scattering of Radio Waves by an Ionized Gas in
    Thermal Equilibrium in the Presence of a Uniform Magnetic Field,"
    Can. J. Phys., Vol. 39, pp. 716-740.

Feldstein, Y. I. and G. V. Starkov (1967), "Dynamics of Auroral Belt and
    Polar Geomagnetic Disturbances," Planet. Space Sci., Vol. 15,
    pp. 209-229.

Gordon, W. E. (1958), "Incoherent Scattering of Radio Waves by Free
    Electrons with Applications to Space Exploration by Radar," Proc. IRE,
    Vol. 46, No. 11, pp. 1824-1829.

Hagfors, T. (1961), "Density Fluctuations in a Plasma in a Magnetic Field,
    with Applications to the Ionosphere," J. Geophys. Research, Vol. 66,
    pp. 1699-1712.

Hays, P. B., R. A. Jones, and M. H. Rees (1973), "Auroral Heating and
    the Composition of the Neutral Atmosphere," Planet. Space Sci.,
    Vol. 21, pp. 559-573.

Jacchia, L. G. (1971), Special Report 332, Res. Space Sci., Smithsonian
    Institution Astrophysics Observatory.

Jones, R. A. and M. H. Rees (1973), "Time Dependent Studies of the
    Aurora--I. Ion Density and Composition," Planet. Space Sci.,
    Vol. 21, pp. 537-557.

Moorcroft, D. R. (1963), "On the Power Scattered from Density Fluctuations
    in a Plasma," J. Geophys. Research, Vol. 68, No. 16, pp. 4870-4872.

Nagy, A. F., R. J. Cicerone, P. B. Hays, J. W. Meriwether, A. E. Belon,
    and C. L. Rino (1974), "Simultaneous Measurement of Ion and Neutral
    Motions by Radar and Optical Techniques," Radio Science, Vol. 9,
    No. 2, pp. 315-321.

Oliver, W. L. (1975), "Models of F_1-Region Ion Composition Variations,"
    J. Atmos. and Terr. Phys., Vol. 37, pp. 1065-1076.

127

REFERENCES (continued)

Rees, M. H. (1975), "Magnetospheric Substorm Energy Dissipation in the
Atmosphere," Planet. Space Sci., Vol. 23, pp. 1589-1596.

Rees, M. H., R. A. Jones, and J. C. G. Walker (1971), "The Influence of
Field-Aligned Currents on Auroral Electron Temperatures," Planet.
Space Sci., Vol. 19, pp. 313-325.

Rees, M. H. and J. C. G. Walker (1968), "Ion and Electron Heating by
Auroral Electric Fields," Ann. Geophys., Vol. 24, pp. 193-199.

Rino, C. L. (1972), "Radar Measurement of Ionosphere Motion in the Pre-
sence of Current-Induced Spectral Asymmetries," Radio Science,
Vol. 7, No. 11, pp. 1049-1060.

Roble, R. G. (1977), "The Thermosphere." In The Upper Atmosphere and
Magnetosphere, Studies in Geophysics, National Academy of Sciences,
Washington, D. C.

Salpeter, E. E. (1961), "Plasma Density Fluctuations in a Magnetic Field,"
Phys. Ref., Vol. 122, pp. 1663-1674.

Schunk, R. W., P. M. Banks, and W. J. Raitt (1976), "Effects of Electric
Fields and Other Processes Upon the Nighttime High-Latitude F Layer,"
J. Geophys. Research, Vol. 81, pp. 3271-3282.

Schunk, R. W. and P. M. Banks (1975), "Auroral N_2 Vibrational Excitation
and the Electron Density Trough," Geophys. Res. Letters, Vol. 2,
No. 6, pp. 239-242.

Schunk, R. W., W. J. Raitt, and P. M. Banks (1975), "Effect of Electric
Fields on the Daytime High-Latitude E and F Regions," J. Geophys.
Research, Vol. 80, No. 22, pp. 3121-3130.

Schunk, R. W. and J. C. G. Walker (1973), "The Theory of Charged Particle
Temperatures in the Upper Atmosphere," in Progress in High Tempera-
ture Physics and Chemistry, C. A. Rouse, ed., pp. 1-62, Pergamon
Press, New York, N.Y.

Singleton, R. C. (1969), "An Algorithm for Computing the Mixed Radix Fast
Fourier Transform," IEEE Trans. on Audio and Electroacoustics, Vol.
AU-17, pp. 93-102.

Swider, W. and R. S. Narcisi (1974), "Ion Composition in an IBC Class II
Aurora," J. Geophys. Research, Vol. 79, pp. 2849-2852.

128

REFERENCES (concluded)

Vallance Jones, A. (1974), Aurora, Chap. 5, D. Reidel Publishing Company, Boston, MA.

Waldteufel, P. (1971), "On the Analysis of High Altitude Incoherent Scatter Data," Report AO 30, Arecibo Observatory, Puerto Rico.

Walls, F. L. and G. H. Dunn (1974), "Measurement of Total Cross Sections for Electron Recombination with NO^+ and O_2^+ Using Ion Storage Techniques," J. Geophys. Research, Vol. 79, pp. 1911-1915.

Walker, J. C. G. and M. H. Rees (1968), "Ionospheric Electron Densities and Temperatures in Aurora," Planet. Space Sci., Vol. 16, pp. 459-475.

Wand, R. H. (1970), "Electron-to-Ion Temperature Ratio from Radar Thomson Scatter Observations," J. Geophys. Research, Vol. 75, pp. 829-838.

Wickwar, V. B. and J. Meriwether (1978), Private communication.

Wickwar, V. B., M. J. Baron, and Robert D. Sears (1975), "Auroral Energy Input from Energetic Electrons and Joule Heating at Chatanika," J. Geophys. Research, Vol. 80, No. 31, pp. 4364-4367.

Wickwar, V. B. (1974), "Analysis Techniques for Incoherent-Scatter Data Interpretation in the 100-to-300 km Region," Technical Report 3, Contract DNA001-72-C-0076, Stanford Research Institute, Menlo Park, California.

GENERAL REFERENCES

Akasofu, S. I. (1977), *Physics of Magnetospheric Substorms*, D. Reidel
    Publishing Company, Dordrecht, Holland.

Bevington, P. R. (1969), *Data Reduction and Error Analysis for the*
    Physical Sciences, McGraw-Hill Book Company, New York, N.Y.

Krall, N. A. and A. W. Trivelpiece (1973), *Principles of Plasma Physics*,
    McGraw-Hill Book Company, New York, N.Y.

Rishbeth, H. and O. Garriott (1969), *Introduction to Ionospheric Physics*,
    Academic Press, New York, N.Y.

Whitten, R. C. and I. G. Poppoff (1971), *Fundamentals of Aeronomy*, John
    Wiley and Sons, Inc., New York, N.Y.